Article

The Different Photoisomerization Efficiency of Azobenzene in the Lowest n#* and ##* Singlets: The Role of a Phantom State

Irene Conti, Marco Garavelli, and Giorgio Orlandi

J. Am. Chem. Soc., **2008**, 130 (15), 5216-5230 • DOI: 10.1021/ja710275e • Publication Date (Web): 13 March 2008

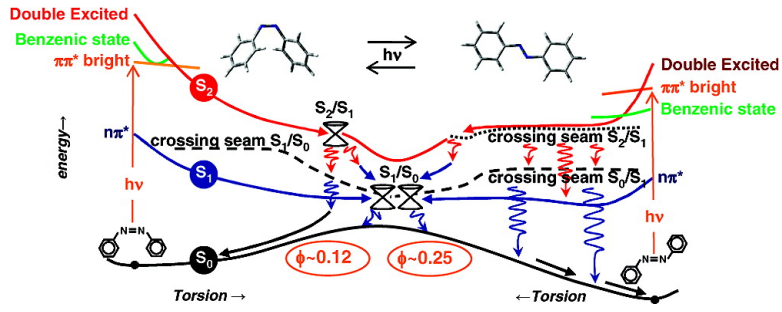

More About This Article

Additional resources and features associated with this article are available within the HTML version:

- Supporting Information
- Links to the 2 articles that cite this article, as of the time of this article download
- Access to high resolution figures
- Links to articles and content related to this article
- Copyright permission to reproduce figures and/or text from this article

View the Full Text HTML

J|A|C|S
ARTICLES

Published on Web 03/13/2008

The Different Photoisomerization Efficiency of Azobenzene in the Lowest nπ^* and $\pi\pi^*$ Singlets: The Role of a Phantom State

Irene Conti,[†] Marco Garavelli,*[,†] and Giorgio Orlandi*[,†,‡]

Department of Chemistry "G. Ciamician", University of Bologna, Bologna, Italy, and INSTM, UdR Bologna, Italy

Received November 13, 2007; E-mail: marco.garavelli@unibo.it; giorgio.orlandi@unibo.it

Abstract: Azobenzene $E \leftrightharpoons Z$ photoisomerization, following excitation to the bright S($\pi\pi^*$) state, is investigated by means of ab initio CASSCF optimizations and perturbative CASPT2 corrections. Specifically, by elucidating the S($\pi\pi^*$) deactivation paths, we explain the mechanism responsible for azobenzene photoisomerization, the lower isomerization quantum yields observed for the S($\pi\pi^*$) excitation than for the S_1(nπ^*) excitation in the isolated molecule, and the recovery of the Kasha rule observed in sterically hindered azobenzenes. We find that a doubly excited state is a photoreaction intermediate that plays a very important role in the decay of the bright S($\pi\pi^*$). We show that this doubly excited state, which is immediately populated by molecules excited to S($\pi\pi^*$), drives the photoisomerization along the torsion path and also induces a fast internal conversion to the S_1(nπ^*) at a variety of geometries, thus shaping (all the most important features of) the S($\pi\pi^*$) decay pathway and photoreactivity. We reach this conclusion by determining the critical structures, the minimum energy paths originating on the bright S($\pi\pi^*$) state and on other relevant excited states including S_1(nπ^*), and by characterizing the conical intersection seams that are important in deciding the photochemical outcome. The model is consistent with the most recent time-resolved spectroscopic and photochemical data.

1. Introduction

Azobenzene (Ab) exists in two different forms, *cis* (*Z*) and *trans* (*E*), which may interconvert both thermally and photochemically.[1–4] Since the two isomers exhibit well-separated absorption bands in the UV–visible region and different physical properties, such as dielectric constant and refractive index, Ab and its derivatives are good candidates for many applications as light-triggered switches,[4] constituents of erasable holographic data, image storage devices, materials with photomodulable properties,[5–8] and in biology.[9] The large photoinduced structural change of this molecule was successfully used to control the helix content in a short peptide[10] and to optically trigger the folding reaction in a peptide ring.[11] For these reasons, the photophysical and photochemical properties of Ab are the subject of a widespread interest.

In the *E* isomer, the molecule is essentially planar, whereas in the *Z* form, the benzene rings are twisted around the C−N bonds to minimize steric repulsion. Therefore, the *Z* form is less stable than the *E* form by 0.6 eV,[12] and at room temperature, it relaxes back thermally to the *E* isomer within several hours by overcoming a barrier of 1.0 eV.[12] The two isomers can be interchanged easily by optical excitation with light at suitable wavelengths.

The absorption spectrum of both *E* and *Z* forms of Ab shows a weak band in the visible region and an intense band in the near-UV spectral region. In hexane solution at room temperature, the weak ($\epsilon_{max} = 400$ L mol^{-1} cm^{-1}) band and the strong ($\epsilon_{max} = 22\,300$ L mol^{-1} cm^{-1}) band of the *E* isomer have the peaks at 432 and 318 nm,[4,13–16] respectively. The *former* band is structureless even in low temperature mixed crystals[17,18] and is attributed to the lowest singlet state of nπ^* type, which belongs to the B_g species of the C_{2h} symmetry group. The *second* band, which shows a rich vibronic structure both in dibenzyl crystals at 20 K[18] and vapor phase at 425 K,[19] is attributed to the $\pi\pi^*$

[†] University of Bologna.
[‡] INSTM.

(1) Zimmermann, G.; Chow, L. Y.; Park, U. I. *J. Am. Chem. Soc.* **1958**, *80*, 3528.
(2) (a) Fischer, E. *J. Am. Chem. Soc.* **1960**, *82*, 3249. (b) Fischer, E.; Malkin, S. *J. Phys. Chem.* **1962**, *66*, 2482.
(3) Rau, H.; Luddeke, E. *J. Am. Chem. Soc.* **1982**, *104*, 1616.
(4) Rau, H. In *Photocromism, Molecules and Systems*; Dürr, H., Bounas-Laurent, H., Eds.; Elsevier: Amsterdam, 1990; Vol. 1, Chapter 4, pp 165–192..
(5) Ikeda, T.; Tsutsumi, O. *Science* **1995**, *268*, 1873.
(6) (a) Willner, I.; Rubin, S.; Riklin, A. *J. Am. Chem. Soc.* **1995**, *113*, 3321. (b) Shipway, A. N.; Willner, I. *Acc. Chem. Res.* **2001**, *34*, 421.
(7) Liu, Z. F.; Hashimoto, K.; Fujishima, K. *Nature* **1990**, *347*, 658.
(8) (a) Balzani, V.; Credi, A.; Marchioni, F.; Stoddard, J. F. *Chem Commun.* **2001**, 1860. (b) Ballardini, R.; Balzani, V.; Credi, A.; Gandolfi, M. T.; Venturi, M. *Acc. Chem. Res.* **2001**, *34*, 445. (c) Balzani, V.; Credi, A.; Venturi, M. *Coord. Chem. Rev.* **1998**, *171*, 3.
(9) Hugel, T.; Holland, N. B.; Cattani, A.; Moroder, L.; Seitz, M.; Gaub, H. E. *Science* **2002**, *296*, 1103.
(10) Flint, D. G.; Kumita, J. R.; Smart, O. S.; Woolley, G. A. *Chem. Biol.* **2002**, *9*, 391.
(11) Spörlein, S.; Carstens, H.; Satzger, H.; Renner, C.; Behrendt, R.; Moroder, L.; Tavan, P.; Zinth, W.; Wachtveitl, J. *Proc. Natl. Acad. Sci. U.S.A.* **2002**, *99*, 7998.
(12) Brown, E. V.; Grunneman, G. R. *J. Am. Chem. Soc.* **1975**, *97*, 621.
(13) Rau, H. *Angew. Chem., Int. Ed. Engl.* **1973**, *12*, 224.
(14) Lednev, I. K.; Ye, T. Q.; Matousek, P.; Townie, M.; Foggi, P.; Neuwahl, F.; Umapathy, S.; Hester, R.; Moore, J. *Chem. Phys. Lett.* **1998**, *290*, 68.
(15) Nagële, T.; Hoche, R.; Zinth, W.; Wachtveitl, J. *J. Chem. Phys.* **1997**, *106*, 519.
(16) Lednev, I. K.; Ye, T. Q.; Hester, R.; Moore, J. *J. Phys. Chem.* **1996**, *100*, 13338.

 10.1021/ja710275e CCC: $40.75

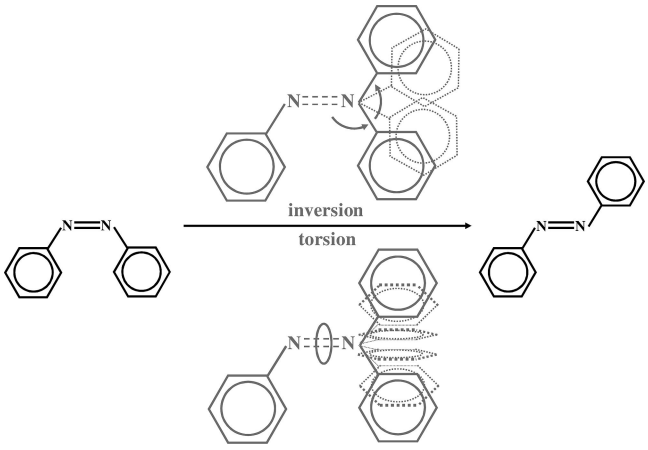

Figure 1. Structures of *E* and *Z* forms of azobenzene with the possible $E \rightarrow Z$ and $Z \rightarrow E$ isomerization paths.

singlet state of B_u symmetry type and is reminiscent of the $S_1 \leftarrow S_0$ transition in stilbene.

Similarly, in the UV–visible absorption spectrum of the *Z*-azobenzene (*Z*-Ab) isomer in hexane, one finds two bands peaked at 440 and 290 nm, with an analogous intensity ratio as in *E*-Ab.[4] While in stilbene the $E \leftrightarrows Z$ isomerization can occur only via torsion of the C═C bond, in Ab, it can proceed along two pathways, the torsion around the *N*═N double bond and the in-plane inversion of one of the CNN angles (see Figure 1). In the latter case, the transition state corresponds to a semilinear structure whereby one nitrogen atom is sp-hybridized.

An unusual property of the $Z \leftrightarrows E$ photoisomerization of Ab is the dependence of the quantum yields on the excitation wavelength.[1–4] In inert solvents, such as *n*-hexane, the quantum yields of the $E \rightarrow Z$ ($Z \rightarrow E$) photoconversion are 0.40/0.12 (0.53/0.25) exciting the $n\pi^*/\pi\pi^*$ states,[20,21] respectively. In other solvents,[3,22] the quantum yields show a similar trend. The different photoisomerization quantum yields in S($n\pi^*$) and S($\pi\pi^*$) represent a case of violation of the Kasha rule.

Surprisingly, the Kasha rule is obeyed in sterically hindered azobenzenes, such as the azobenzenophanes (Ab-phanes), where the motion of each Ab molecule is somewhat affected and hindered by the companion molecule[3,4] and in azobenzene capped crown ether.[22] In his pioneering work,[3,4] Rau proposed that the $E \rightarrow Z$ photoisomerization of the free molecule follows different paths in the $n\pi^*$ and $\pi\pi^*$ states, namely, CNN inversion and *N*═N torsion, respectively. Furthermore, assuming that *only the torsion* motion is frozen in sterically hindered Ab, he suggested that the $\pi\pi^*$ state decays first to S($n\pi^*$), where the photoisomerization occurs. In this way, he explained the observed *different* quantum yields for the excitation in the two bands at 430 and 300 nm in the free Ab and the *equal* quantum yields found in hindered Ab. However, not all the above assumptions are supported by recent theoretical results and by experimental evidence. In particular, attributing the S_1 photoisomerization to the inversion pathway is in contrast with recent calculations[23–26] and with fluorescence anisotropy measurements in inert solvent.[27]

The debate about the photoisomerization mechanism that is dominant in the S($n\pi^*$) and S($\pi\pi^*$) excited states and about the effect produced by the constraints imposed in hindered Ab molecules has been central in subsequent discussions of Ab photochemistry (vide infra). In this respect, it is surprising that even in stilbeno-phanes, where the inversion pathway is not available, the photoisomerization was observed.[28] This finding implies that the torsion path is not inhibited in hindered stilbenes and, by the same token, in hindered Ab, and that molecules have unsuspected abilities to follow their reaction paths under constraints by suitable deformations.

Ultrafast UV–visible absorption spectroscopy and time-resolved fluorescence experiments have provided important clues to unravel the mechanisms of the photophysical and photochemical decay in Ab. Several groups have studied by time-resolved techniques absorption and fluorescence of *E*-Ab and *Z*-Ab following excitation on the $n\pi^*$ state.[14,29–31] The results obtained on the *E*-Ab S($n\pi^*$), neglecting the small dependence on the solvents and on the excitation wavelengths, converge to the following picture: the S($n\pi^*$) decay is described by three exponentials with lifetimes of $\tau_1 \approx 0.30$ ps, $\tau_2 \approx 2.6$ ps, and $\tau_3 \approx 12$ ps. The shortest process is assigned to the relaxation from the Franck–Condon to the equilibrium structure, while τ_2 is attributed to the motion toward the funnels, that is, the conical intersections (CIs), leading to the decay to S_0 and to isomerization. The slowest process is identified with the vibrational cooling in the S_0 state resulting from energy transfer from the Ab molecule to the solvent. This process, which was studied by time-resolved infrared spectroscopy, is estimated to take place on a time scale of ~20 ps.[32]

Transient absorption experiments[29] following excitation of the *Z* isomer on the 435 nm band showed a fast decay with a dominant component with a time constant of 0.17 ps in ethanol and a slower, but weaker, component with time constants of ~1 ps.[29,31,33] Diau and co-workers[27] studied the anisotropy of the S($n\pi^*$) fluorescence of *E*-Ab in two solvents of different viscosity and proposed that the S($n\pi^*$) photoisomerization path follows the *N*═N torsion and the *symmetric* inversion mechanism in hexane and ethylene glycol, respectively. As noted above, the predominance of the torsion mechanism for the S($n\pi^*$) photoisomerization was supported by a number of calculations.[23,25–27] In particular, CASSCF and CASPT2 methods have provided a detailed picture of the S($n\pi^*$) MEP, which was found to follow the torsion path in both Ab isomers[25] and has revealed the key role of twisted CIs in the S($n\pi^*$) decay.

Recently, most of the interest in Ab photochemistry has moved toward elucidating the deactivation of the bright S($\pi\pi^*$)

(17) Hochstrasser, R. M.; Lower, S. K. *J. Chem. Phys.* **1962**, *36*, 3505.
(18) Dick, R. H.; McClure, D. S. *J. Chem. Phys.* **1962**, *36*, 2326.
(19) (a) Andersson, J. A.; Petterson, R.; Tegner, L. *J. Photochem.* **1982**, *20*, 17. (b) Biancalana, A.; Campani, E.; Di Domenico, G.; Gorini, G.; Iacoponi, A.; Masetti, G. *Spectrochim. Acta Part A* **1999**, *55*, 2883.
(20) Bortolus, P.; Monti, S. *J. Phys. Chem.* **1979**, *83*, 648.
(21) Siampiringue, N.; Guyot, G.; Bortolus, P.; Monti, S. *J. Photochem.* **1987**, *37*, 185.
(22) Rau, H. *J. Photochem.* **1984**, *26*, 221.
(23) Cattaneo, P.; Persico, M. *Phys. Chem. Chem. Phys.* **1999**, *1*, 4739.
(24) Ciminelli, C.; Granucci, G.; Persico, M. *Chem.—Eur. J.* **2004**, *10*, 2327.
(25) Cembran, A.; Bernardi, F.; Garavelli, M.; Gagliardi, L.; Orlandi, G. *J. Am. Chem. Soc.* **2004**, *126*, 3234.
(26) Diau, E. W.-G. *J. Phys. Chem. A* **2004**, *108*, 950.
(27) Chang, C. W.; Lu, Y.-C.; Wang, T.-T.; Diau, E. W.-G. *J. Am. Chem. Soc.* **2004**, *126*, 3234.
(28) Tanner, D.; Wennerstrom, O. *Tetrahedron Lett.* **1981**, *22*, 2313.
(29) Nagële, T.; Hoche, R.; Zinth, W.; Wachtveitl, J. *Chem. Phys. Lett.* **1997**, *272*, 489.
(30) Lu, Y.-C.; Chang, C. W.; Diau, E. W.-G. *J. Chin. Chem. Soc.* **2002**, *49*, 693.
(31) Satzger, H.; Sporlein, S.; Root, C.; Wachtveitl, J.; Zinth, W.; Gilch, P. *Chem. Phys. Lett.* **2003**, *372*, 216.
(32) Hamm, P.; Ohline, S. M.; Zinth, W. *J. Chem. Phys.* **1997**, *106*, 519.
(33) Satzger, H. S.; Root, C.; Braun, M. *J. Phys. Chem. A* **2004**, *108*, 6265.

state. The alternative routes for $\pi\pi^*$ de-excitation are (i) the isomerization on the S($\pi\pi^*$) potential energy surface (PES) itself followed by a fast decay to S_0 and (ii) a fast internal conversion from the S($\pi\pi^*$) to the S(nπ^*) state, possibly via intermediate states, followed by isomerization in the vibrationally excited nπ^* state. In the case (ii), the reduced isomerization quantum yield observed for S($\pi\pi^*$) in comparison with that of S(nπ^*) excitation can be accounted for either by invoking a *partial* S($\pi\pi^*$)→S(nπ^*) conversion or by assuming a smaller isomerization yield for the hot S(nπ^*) than for the cold S(nπ^*) state.

In this respect, the time-resolved experiments performed in the past years have provided a wealth of new information. For *E*-Ab in hexane, Lednev et al.[14,16] observed, after S($\pi\pi^*$) excitation, two transient bands at ~475 nm (τ_1 < 0.2 ps) and ~400 nm (τ_2 ~1 ps) and a weaker band around ~400 nm with a lifetime of τ_3 ~16 ps, while Tahara and co-workers[34] measured the lifetimes of the fluorescence emitted from the S($\pi\pi^*$) (τ ~ 0.11 ps) and S(nπ^*) (τ ~ 0.50 ps) states. They recorded also the transient Raman and absorption spectra[35] upon excitation of both $\pi\pi^*$ and nπ^* states and found that the spectra of the two states were practically identical. Thus, they proposed that excitation to S($\pi\pi^*$) is immediately followed by decay to S(nπ^*) and that the isomerization path for the $\pi\pi^*$ and nπ^* excitations is the same and should be identified with the inversion coordinate.[36] Furthermore, they explained the reduced isomerization quantum yield of S($\pi\pi^*$) by assuming that the vibrationally hot S(nπ^*) state produced in the S($\pi\pi^*$)→S(nπ^*) conversion decays to S_0 at the inverted as well as at the reactant geometries with loss of isomerization yield.[36]

More recently, Braun and co-workers[33] measured the transient absorption spectra of *E*-Ab and of *Z*-Ab excited to S($\pi\pi^*$) in ethanol solvent. They identified for *E*-Ab four time constants: $\tau_1 = 0.13$ ps, $\tau_2 = 0.42$ ps, $\tau_3 = 2.9$ ps, and $\tau_4 = 12.0$ ps, which were attributed to the vibrational relaxation in S($\pi\pi^*$), to the decay times of S($\pi\pi^*$) and of S(nπ^*), and to the vibrational cooling in S_0, respectively. Three time constants were extracted from the *Z*-Ab transient absorption spectrum: $\tau_1 = 0.2$ ps, $\tau_2 = 1.1$ ps, and $\tau_3 = 14.0$ ps, which describe the decay of S($\pi\pi^*$) and S(nπ^*) states and the vibrational cooling in S_0, respectively. Since, except for τ_1, the other time constants of the *E* isomer are very similar to the lifetimes observed for the nπ^* excitation, Braun et al.[33] concluded that the decay of the $\pi\pi^*$ state can be described by a two-step process, namely, S($\pi\pi^*$)→S(nπ^*) and S(nπ^*)→S_0, and that the isomerization process takes place on the S(nπ^*) PES. These authors explained the Kasha rule failure by assuming that photoreaction occurs at different S(nπ^*) geometries upon excitation in the two states.

Finally, on the basis of time-resolved photoelectron spectroscopy (TRPES) in supersonic beams, a different and alternative hypothesis was recently suggested by Schultz et al.[37] for the Kasha rule violation, which was assigned to a newly observed benzenic state that can also be populated by initial UV (330 nm) excitation and is assumed to be nonreactive.

Clearly, our understanding of the Ab photoisomerization in S($\pi\pi^*$), occurring on multidimensional PESs, is still incomplete. Very important contributions can be provided by quantum chemical calculations, which can identify the relevant PES, minimum energy paths (MEPs), interstate couplings, and conical intersections that govern the excited state decay. Since the first ab initio study on Ab,[38] based on a STO-3G atomic orbitals, a number of quantum chemical calculations employing up to date methodologies have been performed in the past years to clarify the photochemical behavior of Ab excited in the S($\pi\pi^*$) state.[23,24,39–41]

The results of CIPSI[23] and CASSCF[39] calculations at the ground-state-optimized potential energy curve (PEC) revealed that the photoisomerization on the $^1\pi\pi^*$ state can occur only on the torsion coordinate and that an excited state of A symmetry type with a PEC showing a pronounced minimum at 90° may be involved in the photoisomerization process. However, the nature of this A-type state, which at 90° is at lower energy than the bright S($\pi\pi^*$) state, is not univocally defined in the two calculations, and its precise role in the photoreactivity is not specified. Ishikawa et al.[40] calculated at the CASSCF level the two-dimensional torsion/inversion PES of the S(nπ^*), S($\pi\pi^*$), and S($n^2\pi^{*2}$) lowest singlet excited states and suggested that the isomerization from S($\pi\pi^*$) should proceed by decay to S(nπ^*) or via the intermediate S($n^2\pi^{*2}$). In these studies, optimized excited state PESs and MEPs were not computed and a comprehensive explanation of the main features of the S($\pi\pi^*$) photoisomerization was not attempted, leaving the mechanism of the S($\pi\pi^*$) photoisomerization still uncertain.

Recently, an ab initio CASPT2//CASSCF calculation has been performed on a molecule akin to Ab, cyclohexenylphenyldiazene (CPD), which has a smaller π electron system, as two C=C double bonds of one benzene ring have been saturated by hydrogen atoms.[42] The photoisomerization quantum yields for the excitation of the two bands follow the same pattern found in Ab, but unfortunately, no time-resolved measurement has been made on this system and no information is available on the dynamics of the deactivation processes. From the calculations on the *E* isomer of CPD, including all of the π and n orbitals,[42] it emerges that, after the excitation on the S($\pi\pi^*$) state, the deactivation leads to a state based on the $\pi^2\pi^{*2}/n^2\pi^{*2}$ doubly excited configuration that has a minimum at the twisted geometry.

In this paper, we address the processes of decay and the photoisomerization of Ab excited on the S($\pi\pi^*$) state by ab initio CASPT2//CASSCF calculation. We determine the critical structures, minima and CIs, and the MEP originating on the bright S($\pi\pi^*$) and on other relevant excited states including the S_1(nπ^*) state, and we find the seams of conical intersections that are important in deciding the photochemical outcome. We provide a novel S($\pi\pi^*$) deactivation model, based on the $\pi_{N=N}\pi_{N=N} \rightarrow \pi^*_{N=N}\pi^*_{N=N}$ configuration, that accounts for the different quantum yields observed for Ab and for hindered Ab, in agreement with the information revealed by MD simulations[24,43–46] and experimental results available on hindered systems,[3,22,47–50] and elucidates the observed time-resolved spectra.

(34) Fujino, T.; Arzhantsev, S. Yu.; Tahara, T. *J. Phys. Chem. A* **2001**, *105*, 8123.
(35) Fujino, T.; Tahara, T. *J. Phys. Chem. A* **2000**, *104*, 4203–4210.
(36) Fujino, T.; Arzhantsev, S. Yu.; Tahara, T. *Bull. Chem. Soc. Jpn.* **2002**, *75*, 1031.
(37) Schultz, T.; Quenneville, J.; Levine, B.; Toniolo, A.; Martinez, T. J.; Lochbrunner, S.; Schmitt, M.; Shaffer, J. P.; Zgierski, M. Z.; Stolow, A. *J. Am. Chem. Soc.* **2003**, *125*, 8098.
(38) Monti, S.; Orlandi, G.; Palmieri, P. *Chem. Phys.* **1982**, *71*, 87.
(39) Gagliardi, G.; Orlandi, G.; Bernardi, F.; Cembran, A.; Garavelli, M. *Theor. Chem. Acc.* **2004**, *111*, 363.
(40) Ishikawa, T.; Noro, T.; Shoda, T. *J. Chem. Phys.* **2001**, *115*, 7503.
(41) Fliegl, H.; Kohn, A.; Hattig, C.; Alrichs, R. *J. Am. Chem. Soc.* **2003**, *125*, 9821.
(42) Conti, I.; Marchioni, F.; Credi, A.; Orlandi, G.; Rosini, G.; Garavelli, M. *J. Am. Chem. Soc.* **2007**, *129*, 3198.

Table 1. Observed and Calculated Energies of the Lowest $S_0 \rightarrow S(n\pi^*)$ and $S_0 \rightarrow S(\pi\pi^*)$ Transitions

Absorption							
E-Ab	ΔE, 10^3 cm^{-1} (kcal/mol)	λ_{max} (nm)	ΔE_{calcd},[a] 10^3 cm^{-1} (kcal/mol)	*Z*-Ab	ΔE, 10^3 cm^{-1} (kcal/mol)	λ_{max} (nm)	ΔE_{calcd},[a] 10^3 cm^{-1} (kcal/mol)
$S_0 \rightarrow S_1(n\pi^*)$	23.15	432	20.39	$S_0 \rightarrow S_1(n\pi^*)$	22.73	440	21.93
vert.[b]	66.2		58.3	vert.[b]	65.0		62.7
$S_0 \rightarrow S_1(n\pi^*)$	22.72	440	20.39	$S_0 \rightarrow S_1(n\pi^*)$	23.53	425	21.93
vert.[e]	65.0		58.3	vert.[e]	67.3		62.7
$S_0 \rightarrow S_1(n\pi^*)$	19.50	513	16.19				
0–0[b]	55.7		46.3				
$S_0 \rightarrow S_1(n\pi^*)$	18.52	≈540	16.19				
0–0[e]	52.9		46.3				
$S_0 \rightarrow S(\pi\pi^*)$	31.45	318	34.13	$S_0 \rightarrow S(\pi\pi^*)$	34.48	290	38.04
vert.[b]	89.9		97.6	vert.[f]	98.60		108.8
$S_0 \rightarrow S(\pi\pi^*)$[e]	33.20	301	34.13	$S_0 \rightarrow S(\pi\pi^*)$	37.74	265[b]	38.04
vert.	94.9		97.6	vert.[e]	107.9		108.8
$S_0 \rightarrow S(\pi\pi^*)$	28.00	357	31.09				
0–0[b]	80.1		88.9				
$S_0 \rightarrow S(\pi\pi^*)$[c]	27.66	362	31.09				
0–0	79.1		88.9				
$S_0 \rightarrow S(\pi\pi^*)$[d]	30.0	333	31.09				
0–0	85.8		88.9				
$S_0 \rightarrow S(\pi\pi^*)$[e]	29.61	337	31.09				
0–0	84.8		88.9				
Emission							
$S_0 \rightarrow S(\pi\pi^*)$	34.48	290	38.04				
vert.[b]	98.6		108.8				
$S_1(n\pi^*) \rightarrow S_0$	15.00	665	10.25				
vert.[b]	42.9		29.3				
$S(\pi\pi^*) \rightarrow S_0$	25.64	390	27.80				
vert.[b]	73.3		79.5				

[a] Present results from the CASPT2//CASSCF/6-31G* calculations. [b] in hexane solvent, extrapolated, from refs 34 and 36. [c] In dibenzyl single crystal, from ref 18. [d] In isolated molecule, estimated by adding to the dibenzyl crystal $S(\pi\pi^*)-S_0$ energy gap the same crystal red shift (2337 cm^{-1}) observed for the corresponding band of stilbene (see ref. 57). [e] In the gas phase, at 152 °C, from ref 19. [f] In hexane solvent, from ref 4.

2. Computational Details

The PESs for the $E \rightleftarrows Z$ photoisomerization from the $S(\pi\pi^*)$ state have been studied using fully unconstrained optimizations and MEP computations at the CASSCF level[51] (when possible, single state computations have been used; otherwise, when root flipping problems occurred, state average calculations have been the choice), followed by single point CASPT2[52] computations on the optimized relevant structures to account for correlation energy.

The search of CIs was performed by using procedures developed in our laboratory or according to the prescriptions of ref 53. This procedure works by minimizing the two-roots state average (SA) CASSCF energy in the *n*-2-dimensional intersection space (orthogonally to the branching space directions x_1 and x_2) that preserves the degeneracy.

Then, at all the interesting geometries, a state average CASSCF procedure, with equal weights between the involved states of the singlet manifold (the first nine singlet states in *E*-CPD and in *Z*-CPD), has been used to generate molecular orbitals, energies, and the reference functions for subsequent CASPT2 calculations. An imaginary shift[54] of 0.2 ua was employed for all state-averaged CASPT2 computations. This option is used to eliminate intruder state problems. The CASSCF state interaction (CASSI)[51] method has been used to calculate the transition dipole moments. In the formula for the oscillator strength, the CASSCF transition moment and the energy difference obtained at the CASPT2 level have been used. All computations have been performed with the tools available in the Gaussian 03[55] and the MOLCAS-6[56] quantum chemistry programs.

The active space choice is a crucial step in a CASSCF calculation. Here our choice was to include 10 orbitals and electrons of the π system plus the two doubly occupied nitrogen lone pairs, resulting in an active space of 12 orbitals and 14 electrons. A 6-31G* basis set of atomic orbitals was used.

3. Results

3.1. Calculations of the Lowest Excited States at the Ground-State *E* and *Z* Structures. Experimental transition energies pertinent to the two UV and visible bands are collected in Table 1 together with the computed values. The energies of the maxima in absorption and in emission spectra and the extrapolated 0–0 band energy, ΔE_{00}, of *E*- and *Z*-Ab in hexane solution[4,34] are given. For the intense $\pi\pi^*$ band, we show also

(43) Toniolo, A.; Ciminelli, C.; Persico, M.; Martinez, T. J. *J. Chem. Phys.* **2005**, *123*, 234408.
(44) Ciminelli, C.; Granucci, G.; Persico, M. *J. Chem. Phys.* **2005**, *123*, 174317.
(45) Nonnenberg, C.; Gaub, H.; Frank, I. *Chem. Phys. Chem.* **2006**, *7*, 1455.
(46) Granucci, G.; Persico, M. *Theor. Chem. Acc.* **2007**, *117*, 1131.
(47) Pancur, T.; Renth, F.; Temps, F.; Harbaum, B.; Krüger, A.; Herges, R.; Näther, C. *Phys. Chem. Chem. Phys.* **2005**, *7*, 1985.
(48) Lednev, I. K.; Ye, T. Q.; Abbott, L. C.; Hester, R. E.; Moore, J. N. *J. Phys. Chem. A* **1998**, *102*, 9161.
(49) Rau, H.; Waldner, I. *Phys. Chem. Chem. Phys.* **2002**, *4*, 1776.
(50) Bassotti, E.; Carbone, P.; Credi, A.; Di Stefano, M.; Masiero, S.; Negri, F.; Orlandi, G.; Spada, G. P. *J. Phys. Chem. A* **2006**, *110*, 12385.
(51) Roos, B. O. In *Advances in Chemical Physics: Ab Initio Methods in Quantum Chemistry-II*; Lawley, K. P., Ed.; John Wiley & Sons Ltd.: Chichester, England, 1987; Vol. LXIX, p 399.
(52) Malmqvist, P.-A.; Roos, B. O. *Chem. Phys. Lett.* **1989**, *155*, 189.
(53) (a) Ragazos, I. N.; Robb, M. A.; Bernardi, F.; Olivucci, M. *Chem. Phys. Lett.* **1992**, *197*, 217. (b) Bearpark, M. J.; Robb, M. A.; Schlegel, H. B. *Chem. Phys. Lett.* **1994**, *223*, 269.
(54) Försberg, N.; Malmqvist, P.-A.; Roos, B. O. *Chem. Phys. Lett.* **1997**, *274*, 196.
(55) Frisch, M. J.; *Gaussian 98*, revision A.6; Gaussian, Inc.: Pittsburgh, PA, 1998.
(56) Andersson, K.; *MOLCAS*, version 5.2; University of Lund: Lund, Sweden, 2001.

Table 2. Computed Vertical Transition Energies, Wave Functions with the Representation of Molecular Orbitals Involved in the Most Important Configurations, and Oscillator Strengths of the Lowest Excited Singlet States of *E*-Ab at the FC Planar Geometry[a]

E-Azobenzene					
State	Electr. Configurations	Coeff.	Energy CAS-PT2		*f*
			eV	Kcal/mol	
$S_0(1\,^1A_g)$	ground state	0.90	0.00	0.00	
$S_1(1\,^1B_g)$	$n_+ \rightarrow \pi_{N=N}^*$	0.88	2.53	58.3	0
$S_2(1\,^1B_u)$	$\pi_{N=N} \rightarrow \pi_{N=N}^*$	0.83	4.23	97.6	0.616
$S_3(2\,^1B_u)$	$\pi_1 \rightarrow \pi_{N=N}^*$ $\pi_{N=N} \rightarrow \pi_1^*$	0.54 0.30	4.46	102.8	0.070
$S_4(2\,^1A_g)$	$\pi_3 \rightarrow \pi_{N=N}^*$ $\pi_2 \rightarrow \pi_{N=N}^*$	0.45 0.36	4.53	104.5	10^{-9}
$S_5(1\,^1A_u)$	$(\pi_{N=N}\, n_+) \rightarrow (\pi_{N=N}^*)^2$	0.67	4.77	109.9	0.008
$S_6(2\,^1B_g)$	$(\pi_{N=N}\, n_+) \rightarrow (\pi_{N=N}^*)^2$ $n_+ \rightarrow \pi_1^*$	0.50 0.48	5.13	118.3	10^{-12}
$S_7(3\,^1A_g)$	$\pi_2 \rightarrow \pi_{N=N}^*$ $(\pi_{N=N})^2 \rightarrow (\pi_{N=N}^*)^2$	0.45 0.42	5.17	119.3	10^{-10}
$S_8(2\,^1A_u)$	$n_- \rightarrow \pi_{N=N}^*$ $n_+ \rightarrow \pi_2^*$	0.45 0.43	5.69	131.1	10^{-12}

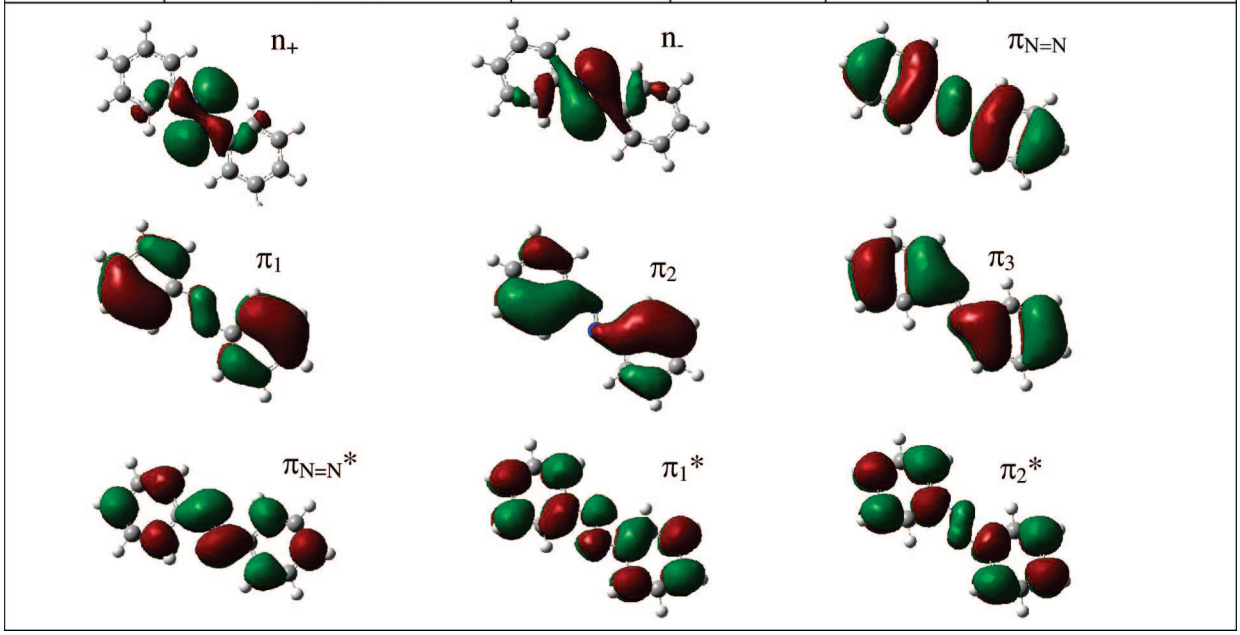

[a] From the CASPT2//CASSCF/12-14/6-31G* calculations.

the ΔE_{00} energy of *E*-Ab in low-temperature dibenzyl crystal[18] and the extrapolated ΔE_{00} in the isolated molecule obtained by correcting for the red shift induced by the crystal matrix. This ΔE_{00} value (85.8 kcal/mol) is in agreement with the energy (85.4 kcal/mol) of the first feature in the vapor spectrum.[19] The calculated ΔE_{00} (88.9) is only 3 kcal/mol higher than the observed values.

Vertical transitions, oscillator strengths (*f*), wave function composition, and oscillator strengths have been computed by CASPT2//CASSCF/6-31G* for the lowest eight excited singlet states in the isolated *E*-Ab and in *Z*-Ab. The results pertinent to the ground-state equilibrium geometry of the *E* and Z isomers, (*E*-MinS_0) and (*Z*-MinS_0), are reported in Tables 2 and 3, respectively, where the nature of electronic states is clarified by their most important electronic configurations. The lowest excited singlet state, S_1, is of $n\pi^*$ type in both isomers.

In the *E*-Ab, $S_1(n\pi^*)$ belongs to the B_g representation, and the computed $S_1(n\pi^*) \leftarrow S_0$ vertical energy gap (58.3 kcal/mol) is lower by 7 kcal/mol than the energy of the first absorption peak, as shown in Table 1. The computed oscillator strength ($\sim$0) is consistent with the forbidden character ($B_g \leftarrow A_g$) of the $S_1 \leftarrow S_0$ transition, which obtains its tiny intensity ($\epsilon = 400\ M^{-1}$

Table 3. Computed Vertical Transition Energies, Wave Functions with the Representation of Molecular Orbitals Involved in the Most Important Configurations, and Oscillator Strengths (*f*) of the Lowest Excited Singlet States of *Z*-Ab at the FC Planar Geometry[a]

Z-Azobenzene					
State	Electronic Configurations	Coeff.	Energy CAS-PT2		*f*
			eV	Kcal/mol	
$S_0(1\,^1A)$	ground state	0.90	0.00	0.00	
$S_1(1\,^1B)$	$n_- \rightarrow \pi_{N=N}^*$	0.84	2.72	62.7	0.015
$S_2(2\,^1B)$	$\pi_3 \rightarrow \pi_{N=N}^*$	0.57	4.49	103.5	0.035
$S_3(2\,^1A)$	$\pi_2 \rightarrow \pi_{N=N}^*$	0.66	4.54	104.6	0.011
$S_4(3\,^1B)$	$n_- \rightarrow \pi_1^*$ $\pi_3 \rightarrow \pi_{N=N}^*$	0.50 0.50	4.72	108.8	0.191
$S_5(4\,^1B)$	$\pi_5 \rightarrow \pi_{N=N}^*$ $\pi_4 \rightarrow \pi_{N=N}^*$ $\pi_2 \rightarrow \pi_2^*$	0.39 0.33 0.31	5.00	115.4	0.004
$S_6(3\,^1A)$	$\pi_4 \rightarrow \pi_{N=N}^*$ $\pi_5 \rightarrow \pi_3^*$	0.39 0.36	5.12	118.0	< 0.001
$S_7(4\,^1A)$	$(n_-)^2 \rightarrow (\pi_{N=N}^*)^2$	0.53	5.41	124.8	0.012
$S_8(5\,^1A)$	$(n_-)^2 \rightarrow (\pi_{N=N}^*)^2$ $(\pi_3\pi_1) \rightarrow (\pi_{N=N}^*)^2$	0.53 0.36	6.06	139.7	0.007

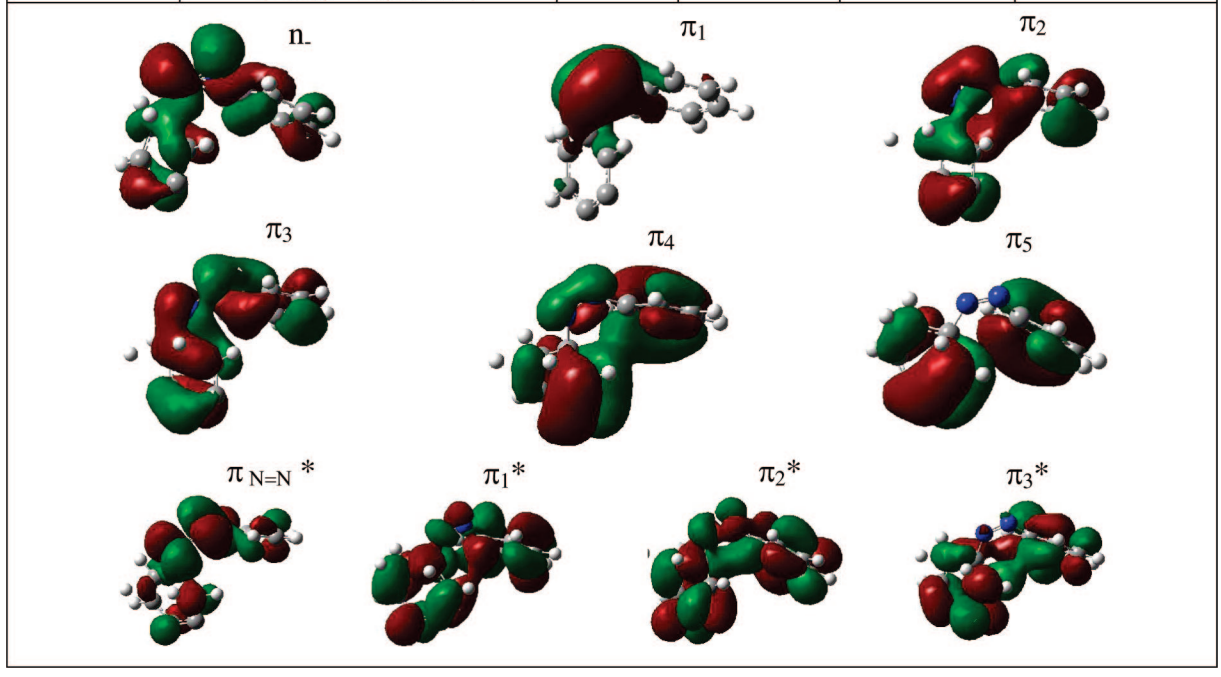

[a] From the CASPT2//CASSCF/12–14/6–31G* calculations.

cm^{-1})[4] in *E*-Ab via out-of-plane vibrations that borrow intensity from allowed $S_0 \rightarrow \pi\pi^*$ transitions.

In the *Z*-Ab isomer, the computed $S_1(n\pi^*)$ belongs to the B representation and the vertical $S_1(n\pi^*) \leftarrow S_0$ transition energy is lower than the energy of the first absorption peak by ca. 4 kcal/mol, as shown in Table 1. The computed oscillator strength, $\sim 10^{-2}$ (reported in Table 2), is in agreement with the weak, but allowed character of the $S_1 \leftarrow S_0$ excitation ($\epsilon = 1250\ M^{-1}\ cm^{-1}$).[4] Our calculation for the isolated molecule appears to underestimate the energies of S_1. One reason is the neglect of the solvent effect which increases the excitation energies of $n\pi^*$ states, as it is well-known.[59]

(57) The $S_1 - S_0$ ΔE_{00} of stilbene in bibenzil crystal (see ref. 18) is 29 903 cm^{-1} and in supersonic beams is 32 240 cm^{-1} (see ref. 58).

(58) (a) Syage, J. A.; Lambert, W. R.; Felker, P. M.; Zewail, A. H.; Hochstrasser, R. M. *Chem. Phys. Lett.* **1982**, *88*, 268. (b) Syage, J. A.; Felker, P. M.; Zewail, A. H. *J. Chem. Phys.* **1984**, *81*, 4685. (c) Amirav, A.; Jortner, J. *Chem. Phys. Lett.* **1983**, *95*, 295.

(59) Klessinger, M.; Michl, J. *Excited States and Photochemistry of Organic Molecules*; VCH: New York, 1995..

The intense band in the visible−UV absorption spectrum is associated with a $\pi\pi^*$ singlet state that is based on the configuration $\pi_{N=N} \rightarrow \pi^*_{N=N}$, in which one electron is promoted from the bonding to the antibonding orbitals that have large components on the N=N group. This state, which is very similar to the lowest singlet state of stilbene, will be in the referred to in the following referred simply as S($\pi\pi^*$).

In *E*-Ab, the S($\pi\pi^*$) state belongs to the B_u representation and, being the second excited state, is assigned as $S_2(B_u)$. The calculated $S_2 \leftarrow S_0$ oscillator strength (0.616) is typical of a strongly allowed transition, in agreement with the experimental value 0.511 estimated by Tahara.[36]

The vertical S($\pi\pi^*$)←S_0 energy gap is overestimated by 7.1 kcal/mol in *E*-Ab and by 6.3 kcal/mol in *Z*-Ab with respect with the hexane solution values. One important reason is the neglect of the solvent effect which decreases the excitation energies of $\pi\pi^*$ states. The overestimate with respect to the gas-phase spectra[19] is less than 3 kcal/mol. The comparison of the 0–0 band energy with the calculated adiabatic energy gap leads to the same conclusions. The calculated adiabatic S($\pi\pi^*$)−S_0 energy gap is 4 kcal/mol higher than the 0–0 band in the gas phase[19] and 3 kcal/mol higher than the 0–0 band of the *E*-Ab 0–0 band in the dibenzyl single crystal corrected by the red shift induced by the crystal, as it is shown in Table 1.

At higher energy, we find for *E*-Ab two benzenic states, $S_3(2B_u)$ and $S_4(2A_g)$, which are 5 and 7 kcal/mol higher than S($\pi\pi^*$), respectively, as shown in Table 2. The oscillator strength of S_3 is found to be modest (0.07), but not negligible.

The next two states, $S_5(A_u)$ and $S_6(B_g)$, of type (nπ^*), are almost degenerate (118.3 and 119.3 kcal/mol) and have negligible oscillator strengths. The following state, $S_7(A_g)$, gets a strong contribution from the doubly excited configuration $\pi_{N=N}\pi_{N=N} \rightarrow \pi^*_{N=N}\pi^*_{N=N}$ in which two electrons are promoted from a bonding to an antibonding orbital with a marked azo character. For this reason, we shall indicate this state as S(DE). In analogy with stilbene, S(DE) is expected to favor the twisted geometry and to play a key role in the photoisomerization of *E*-Ab. Because of its A_g symmetry, the state S(DE) cannot be detected by the ordinary one-photon spectroscopy but could be observed by two-photon spectroscopy. However, we are not aware of any such study.

In *Z*-Ab, the bright S($\pi\pi^*$) state belongs to the B representation and, being the fourth excited state, is assigned as $S_4(B)$, as reported in Table 3. In this isomer, a strict distinction between n and π orbitals does not apply because of the torsion around the C−N and N=N bonds. Thus, both n and $\pi_{N=N}$ orbitals are coupled with benzenic π orbitals. For this reason, the $S_4(B)$ is based on the combination of $\pi \rightarrow \pi^*_{N=N}$ and $n \rightarrow \pi^*$ configurations. The computed $S_4 \leftarrow S_0$ oscillator strength (0.191) is typical of an allowed transition, in agreement with the high measured molar absorption coefficient of ($\epsilon = 5260\ M^{-1}\ cm^{-1}$).[60] A few kcal/mol below this state we find the two benzenic states $S_2(2B)$ and $S_3(2A)$, which have small oscillator strengths. The next two states, $S_5(B)$ and $S_6(A)$, are of mixed nπ^* and $\pi\pi^*$ character and have small (<0.01) oscillator strengths. The following state, $S_7(A)$, has a strong contribution from the doubly excited configuration $nn \rightarrow \pi^*_{N=\ N}\pi^*_{N=N}$ and will be referred to as S(DE). With the N=N torsion, this state evolves into the S(DE) ($\pi_{N=N}\pi_{N=N} \rightarrow \pi^*_{N=N}\pi^*_{N=N}$) state of the *E*-Ab isomer, and it will play an important role in the photoisomerization of *Z*-Ab (vide infra).

The only information available for higher-energy excited states is the vertical transition observed in the gas phase at 5.64 and 4.68 eV for the *E* and *Z* isomer, respectively. In our calculations, we find two states at 6.31 and 6.47 eV for the *E* isomer and two states at 5.44 and 5.94 eV also for the *Z* isomer, with appreciable oscillator strength. In better agreement are the results of the CC2/aug-cc-pVTZ calculations of Ahlrichs and co-workers[61] who report a state with considerable oscillator strength at 5.79 and 4.68 eV for the *E* and *Z* isomers, respectively. At the same time, the CC2 approach does not report states with important contributions from doubly excited configurations, which are important in the photochemical problem we are considering.

3.2. Computational Analysis of the Photoisomerization Induced by $\pi\pi^*$ Excitation. The MEPs of the bright S($\pi\pi^*$) state and of the other states involved in the photoisomerization process, mapping from the ground-state geometry (FC point) of the *E* and *Z* isomers, are summarized in Figures 2 and 3, respectively. In the same figures are shown also the regions of CIs and the critical structures with indication of their most important geometric parameters. The excited-state energies at the critical geometries, obtained at the CASPT2//CASSCF/6-31G* level, are reported in Tables 4 and 5.

In the following, we discuss separately the relaxation and photoisomerization of the two isomers.

3.2.1. Photoisomerization of the *E* Isomer. Deactivation of the $\pi_{N=N} \rightarrow \pi^*_{N=N}$ State. The MEPs of the lower electronic states beginning at the *E* isomer are displayed in Figure 2. Starting from the ground-state equilibrium geometry, the MEP of the "bright" S($\pi\pi^*$) state, S_2, relaxes first to its equilibrium geometry, which is *planar* and, interestingly, does not involve the N=N bond torsion (θ). The $\pi\pi^*$ relaxation entails a skeletal planar rearrangement leading to an increase of N=N bond length and a decrease of C−N bonds, so that all three bonds measure the same length, 1.34 Å. Along the $\pi\pi^*$ MEP, the energy profile of the state S(DE), characterized by the double excitation $\pi_{N=N}\pi_{N=N} \rightarrow \pi^*_{N=N}\pi^*_{N=N}$, which is at higher energy (S_7) at the FC geometry, decreases and crosses the MEP of the bright S($\pi\pi^*$) state. Thus, after the first and fast relaxation step, S(DE) becomes S_2, and the S($\pi\pi^*$) equilibrium geometry coincides with the S(DE)/S($\pi\pi^*$) termend *E*-CI S_3S_2, in Figure 2 and Table 4.

Only after this crossing has occurred, torsion around the N=N bond begins because the MEP energy of S(DE) state, or S_2(DE), decreases slowly with the N=N torsion toward its minimum at the twisted (95°) geometry (MIN-S_2; see Figure 2). We observe that the bright S($\pi\pi^*$) state energy profile does *increase* upon torsion and does not lead to any other efficient decay path except via S_2(DE). In particular, no S($\pi\pi^*$)/S_1(nπ^*) CIs has been found at geometries with reasonably accessible energy. Therefore, after excitation on the bright $\pi\pi^*$ state, molecules relax to an equilibrium planar geometry, then they undergo an ultrafast deactivation to the S_2(DE) state, which thereafter drives the *slow relaxation* toward the twisted geometry, and simultaneously, it drives the *fast internal conversion* to the lower S_1(nπ^*) state at a variety of θ angles.

As shown in Figure 2, from the planar geometry up to $\theta = 123°$, the S_2(DE) MEP (red line) is essentially degenerate with a seam of S_2/S_1 CIs (light red area, from *E*-1-CI S_2S_1 to *E*-2-CI S_2S_1) characterized by the geometrical parameters NN = 1.35

(60) Suzuki, H. *Electronic Absorption Spectra and Geometry of Organic Molecules*; Academic Press: New York, 1967.

(61) Fliegl, H.; Köhn, A.; Hättig, K.; Ahlrichs, R. *J. Am. Chem. Soc.* **2003**, *125*, 9821.

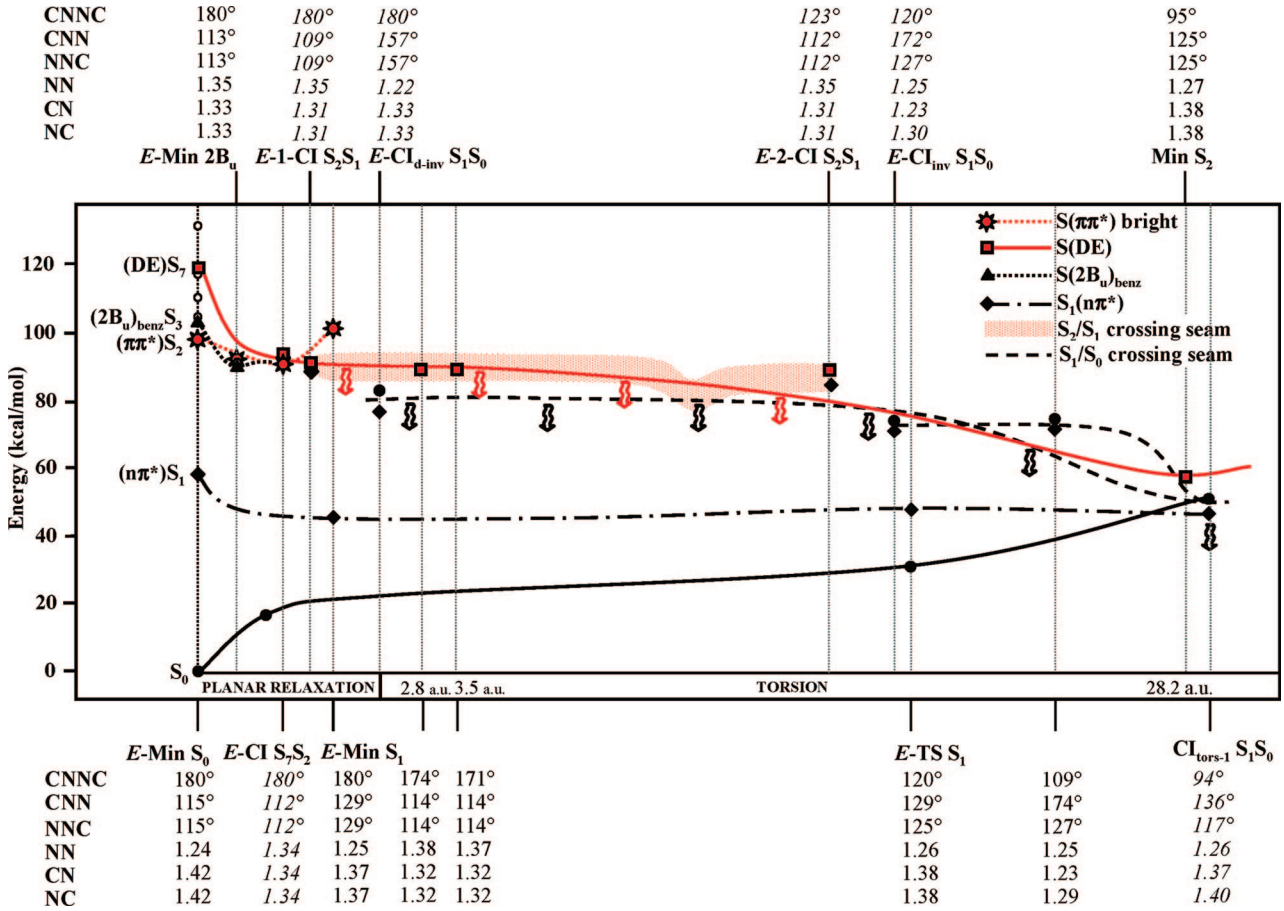

Figure 2. Singlet S($\pi\pi^*$), S(DE), and S$_1$(nπ^*) reaction paths for the $E \rightarrow Z$ photoisomerization in azobenzene. Please note that S(DE) is labeled as S$_7$ at the Franck–Condon geometry, S$_3$ and S$_2$ before and after the crossing with S($\pi\pi^*$), respectively. MEPs and energy profiles have been scaled to match CASPT2 values. Some of the most important structures are indicated, and their most significant geometrical parameters are reported below or above the figure. Red and black arrows show S$_2 \rightarrow$S$_1$ and S$_1 \rightarrow$S$_0$ internal conversion processes, respectively. Black dashed lines represent the extended S$_1$/S$_0$ crossing region whose shape is better shown in Scheme 1. Conical intersection geometries are given in *italics*.

Å, NC = 1.31 Å, and NNC = 109°. We have checked that this S$_1$/S$_2$ crossing seam can be easily reached by moving orthogonally to the S$_2$(DE) MEP along symmetric CNN bending modes, toward smaller CNN/NNC angle values (as indicated by the structure parameters reported in Figure 2), and that this motion is essentially barrierless. Therefore, CNN bending vibrations may provide the excited molecules with an efficient route to enter the S$_2$/S$_1$ crossing seam and to decay to S$_1$ at N=N twisting angles that may be far from 90°.

Since the corresponding geometrical parameters of the S$_1$(nπ^*) equilibrium geometry (*E*-Min S$_1$), NN = 1.25 Å, NC =1.37 Å, and NNC = 129°, are quite different from the parameters of the S$_2$/S$_1$ crossing seam (vide supra), we may infer that NN and NC stretchings and the NNC bending vibrations absorb a substantial amount of the S$_2-$S$_1$ energy difference (about 45 kcal/mol) in the S$_2 \rightarrow$S$_1$ conversion. Therefore, at the time of the S$_2 \rightarrow$S$_1$ crossing, the S$_1$ vibrational energy distribution neither is statistical nor is similar to that obtained in the S$_0 \rightarrow$S$_1$ excitation by the Franck–Condon principle.

Analysis of the S$_1$/S$_0$ Crossing Region. The vibrational energy excess in S$_1$ will be quickly distributed among all the vibrations in ways and with rates that can be clarified only by molecular dynamics calculations. When this process is completed, the vibrational energy distribution will be statistical and little energy will be left to the three coordinates mainly associated with isomerization (N=N twisting, CNN and NNC bendings). That is, the molecules in which vibrational redistribution takes place rapidly in S$_1$ will isomerize in the same way as after the S$_0 \rightarrow$S$_1$ excitation, that is, mainly along the torsion coordinate. However, before the vibrational redistribution in S$_1$ is completed, molecules will have chances to intercept the seam of S$_1$/S$_0$ CIs in the full range $180° > \theta > 94°$, from which a fast decay to S$_0$ occurs. As shown in Figure 2, this seam (black sketched line) is close to S$_2$ and to the S$_2$/S$_1$ crossing region in a large interval of θ values. The S$_1$/S$_0$ crossing region is characterized by a short N=N bond (1.22 Å) and large NNC inversion angles (*E*-CI$_{inv}$ S$_0$S$_1$), both with symmetric (NNC = CNN = 157° for the most stable symmetric S$_0$/S$_1$ CIs, *E*-CI$_{d\text{-}inv}$ S$_0$S$_1$) and nonsymmetric NNC/CNN distortions. To assess the efficiency of the multiple S$_0$/S$_1$ deactivation channel, we have extended further the analysis of the S$_1$/S$_0$ crossing seam, which is schematically depicted in Scheme 1 for the trans isomer.

This crossing space has a symmetric shape with a ridge of *symmetric* bendings (with CNN = NNC) separating a 2-fold channel, each one collecting *nonsymmetric* bending, in which one CNN angle is larger than the other. The topology of this crossing space is substantially identical in the two isomers and spans very different structures, including fully *twisted* geometries, with $\theta \approx 90°$ (CI$_{tors\text{-}n}$ S$_1$/S$_0$), already considered in the analysis of the S$_1$(nπ^*) photoisomerization,[25] the higher-energy *inverted* structures (in which CNN or NNC is (almost) 180°,

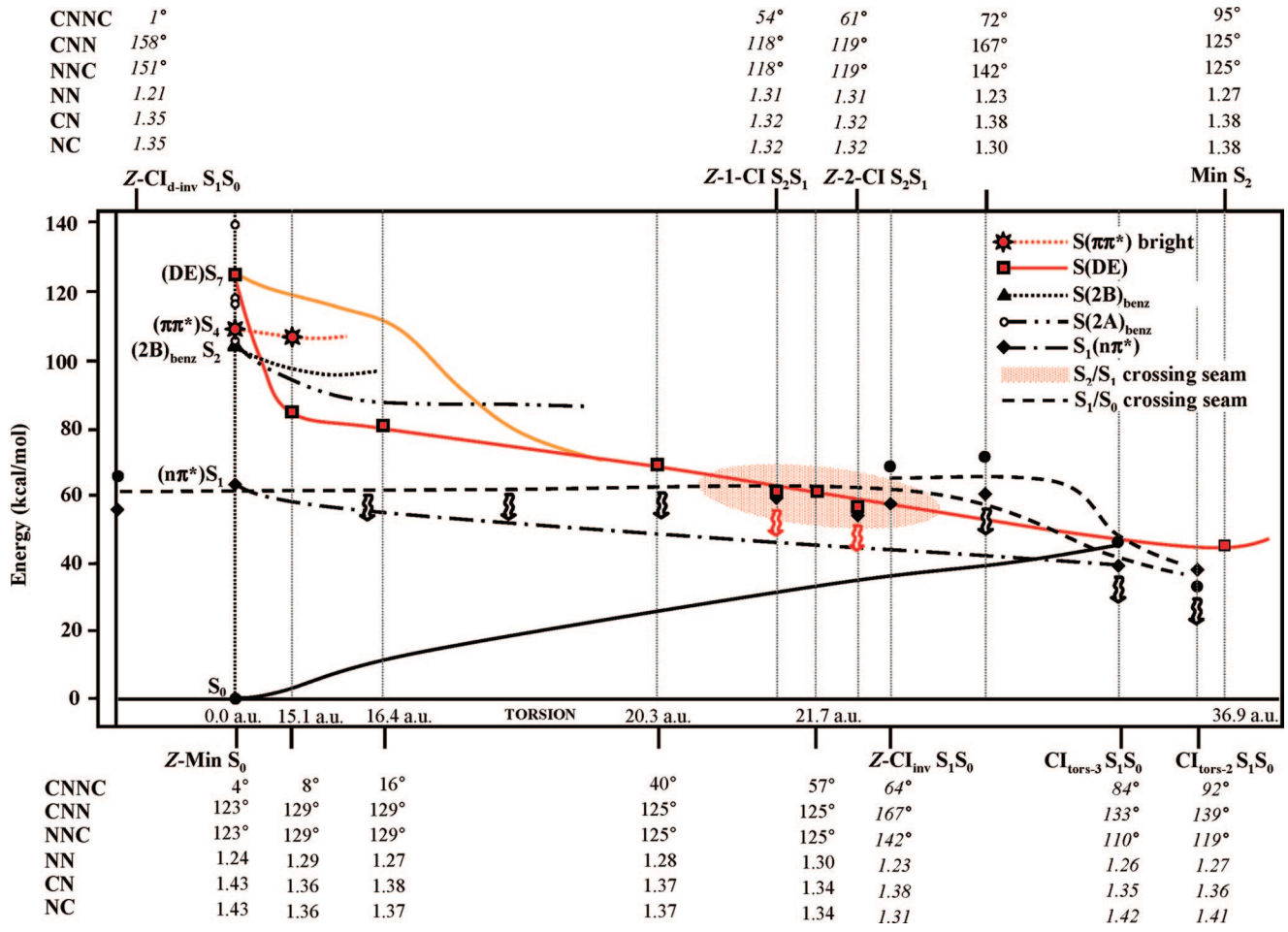

Figure 3. Singlet S($\pi\pi^*$), S(DE), and S_1($n\pi^*$) reaction paths for the $Z \rightarrow E$ photoisomerization in azobenzene. MEPs and energy profiles have been scaled to match CASPT2 values. Orange line shows the S(DE) profiles along the benzenic state (S_2, $(2B)_{benz}$) path. Some of the most important structures are indicated, and their most significant geometrical parameters are reported below or above the figure. Red and black arrows show $S_2 \rightarrow S_1$ and $S_1 \rightarrow S_0$ internal conversion processes, respectively. Black dashed lines represent the extended S_1/S_0 crossing region whose shape is better shown in Scheme 1. Conical intersection geometries are given in *italics*.

associated with the *inversion* mechanism) and *symmetric* bending structures that were discussed by Diau.[26] The symmetric bending CIs are on the ridge of the seam, that is, at the highest energies, while a lower energy is observed for nonsymmetric bending CIs. Anyway, it is worthy to note that a flat high-energy surface exists for both isomers at geometries where the N=N torsion is not involved (i.e., CNNC = 0°/180°), and this makes symmetric/nonsymmetric bending CIs almost isoenergetic. It should also be noted that the CNNC torsion angle loses significance at inversion CIs (a CNN bending angle approaches 180° here), that is, *E*-CI_{inv} (120°) and *Z*-CI_{inv} (64°) would collapse to the same structure for a 180° CNN bending angle. In this respect, the nomenclature *E* or *Z* for this inversion crossing points is just formal as the structure should be unique. Considering also the N=N twisting, the lowest energy CIs are found for θ close to 90°.

For clarity, it should be pointed out that this analysis is based on the CASSCF (two-roots state average) energies employed for the optimization of the S_1/S_0 crossing region. CASPT2 corrections confirm qualitatively the topology displayed in Scheme 1, although sometimes they lead to a non-negligible S_1-S_0 energy gap, revealing that the PT2 crossing seam is slightly displaced with respect to the CAS one. While in general this CASPT2 energy gap (and, consequently, the displacement of CIs) is rather small, there are some structures (such as the *Z*,*E*-$CI_{d\text{-}inv}$ structure) where this problem is more serious. Anyway, *Z*,*E*-$CI_{d\text{-}inv}$ is a high-energy real crossing point at the CASSCF (two-roots state average) level, and the two roots have already swapped at the PT2 level (see Table 4). Thus, the crossing point must also exist at the PT2 level, albeit it is slightly shifted (and much higher in energy than the twisted crossings). In this respect, it must be noted that PT2 energy values are upper limit estimates for the energy of this crossing seam high-energy portion.

In conclusion, while the lowest energy S_1/S_0 CIs are found at twisted structures and are the only ones accessible for cold molecules, very different S_1/S_0 CIs can be *potentially* reached after the $S_2 \rightarrow S_1$ decay at partially twisted, higher-energy regions. Clearly, the molecules that follow the latter channel do not isomerize. The molecules that reach the S_2/S_1 CI seam close to the twisted geometry may isomerize and are the ones that account for the isomerization yield observed upon $\pi\pi^*$ excitation.

3.2.2. Photoisomerization of the *Z* Isomer. Deactivation of the $\pi_{N=N} \rightarrow \pi^*_{N=N}$ State. The MEPs of the lower electronic states beginning at the *Z* isomer are displayed in Figure 3. Starting from the ground-state equilibrium geometry, the MEP of the bright $S_4(\pi\pi^*)$ state (red dotted line, Figure 3) leads toward its equilibrium geometry by a mainly skeletal deformation and a slow energy decrease. Along this path, the energy profile of S_7 (red line), the S(DE) state characterized by the $nn \rightarrow \pi^*_{N=N}\pi^*_{N=N}$

Table 4. CASPT2 and CASSCF Relative (ΔE) Energies for All the Relevant Structures along the Photochemical Paths of the *E* Isomer[a]

		CASPT2		CASSCF
structure	state	ω[b]	ΔE (kcal/mol)	ΔE (kcal/mol)
E-MinS_0	S_0	0.63	0.0	0.0
	S_1	0.62	58.3	73.7
	S_2	0.61	97.6	146.5
	S_3	0.61	102.8	131.6
	S_4	0.61	104.5	131.5
	S_5	0.61	109.9	139.1
	S_6	0.61	118.3	154.4
	S_7	0.61	119.3	148.4
E-Min S_1	S_0	0.63	17.0	16.1
	S_1	0.63	46.3	59.1
E-TS S_1	S_0	0.63	30.7	35.6
	S_1	0.63	47.7	62.0
CI_{tors-1} S_1S_0	S_0	0.63	52.1	61.1
	S_1	0.63	47.4	56.8
CI_{tors-2} S_1S_0	S_0	0.63	50.9	59.3
	S_1	0.63	45.2	56.2
CI_{tors-3} S_1S_0	S_0	0.63	58.7	70.8
	S_1	0.63	51.6	64.6
E-CI_{inv}	S_0	0.63	74.0	87.0
	S_1	0.63	70.3	80.9
E-CI_{d-inv}	S_0	0.63	85.6	92.9
	S_1	0.63	71.0	84.7
E-CI S_3S_2[c]	S_0	0.63	9.0	13.7
	S_1	0.62	64.6	83.1
	S_2	0.61	92.3	129.6
	S_3	0.62	93.4	110.7
E-1-CI S_2S_1	S_1	0.62	88.0	107.7
	S_2	0.62	89.3	107.5
E-2-CI S_2S_1	S_1	0.62	83.9	108.0
	S_2	0.62	88.5	108.2
Min S_2	S_0	0.63	47.7	64.4
	S_1	0.62	38.3	48.5
	S_2	0.62	57.8	76.0
E-Min $2B_u$	S_0	0.63	9.4	15.4
	S_1	0.62	63.8	83.0
	S_2	0.61	88.9	116.4
	S_3	0.61	89.6	114.4
	S_4	0.61	92.5	136.7

[a] Energy values are state average through the first nine singlet states. CI structures were determined by the two-roots state average procedure. The energy for the ground-state minimum is chosen as the zero. Basis set: 6-31G*. Active space: 14 electrons in 12 MOs. [b] The ω is the weight of the dominant CASSCF wave function. [c] S_3 corresponds to the S_7 state of the Min S_0 geometry, that is, to the S(DE) state.

Table 5. CASPT2 and CASSCF Relative (ΔE) Energies for All the Relevant Structures along the Photochemical Paths of the *Z* Isomer[a]

		CASPT2		CASSCF
structure	state	ω[b]	ΔE (kcal/mol)	ΔE (kcal/mol)
Z-MinS_0	S_0	0.63	0.0	0.0
	S_1	0.62	62.7	77.8
	S_2	0.60	103.5	143.4
	S_3	0.61	104.6	126.6
	S_4	0.59	108.8	169.6
	S_5	0.61	115.4	141.6
	S_6	0.61	118.0	142.9
	S_7	0.61	124.8	152.1
CI_{tors-1} S_1S_0	S_0	0.63	39.7	44.3
	S_1	0.63	35.0	40.0
CI_{tors-2} S_1S_0	S_0	0.63	38.5	42.5
	S_1	0.63	32.8	39.4
CI_{tors-3} S_1S_0	S_0	0.63	46.3	54.0
	S_1	0.63	39.2	47.9
Z-CI_{inv} S_1S_0	S_0	0.63	69.0	69.8
	S_1	0.63	56.7	67.2
Z-CI_{d-inv} S_1S_0	S_0	0.63	65.8	68.9
	S_1	0.63	54.9	66.1
Z-1-CI S_2S_1	S_1	0.61	59.4	92.0
	S_2	0.61	60.7	85.7
Z-2-CI S_2S_1	S_1	0.62	57.3	82.0
	S_2	0.62	54.4	81.6
Min S_2	S_0	0.63	35.3	47.7
	S_1	0.62	25.9	31.8
	S_2	0.62	45.4	59.3

[a] Energy values are state average through the first nine singlet states. CI structures were determined by the two-roots state average procedure. The energy for the ground-state minimum is chosen as the zero. Basis set: 6-31G*. Active space: 14 electrons in 12 MOs. [b] The ω is the weight of the dominant CASSCF wave function.

double excitation, decreases quite fast and crosses the MEP of the bright $\pi\pi^*$ state and of the two benzenic states ($(2B)_{benz}$ and $(2A)_{benz}$) becoming the S_2(DE) state, as shown in Figure 3. This crossing occurs at the *Z* structure with $\theta = 8°$, following the lengthening of NN bond (NN = 1.29 Å) and the shortening of CN bonds (CN = 1.36 Å). Therefore, after excitation on the bright $\pi\pi^*$ state, molecules on their way to relax toward the equilibrium geometry undergo an ultrafast deactivation to the S_2(DE) state, which thereafter drives the relaxation to the twisted geometry or to the internal conversion to the lower $S_1(n\pi^*)$ state in the same way as for the *E* isomer.

We have found that the S_2 MEP energy decreases monotonically with torsion until it reaches its minimum at the fully twisted ($\theta = 94°$) geometry (MIN S_2; see Figure 3). In the torsion interval of $50° < \theta < 65°$, a seam of S_1/S_2 CIs (light red area), characterized by the geometrical parameters NN = 1.31 Å, NC = 1.32 Å, and NNC = 119° becomes essentially degenerate with the S_2 MEP.

As in the case of the *E* isomer, molecules can easily access this S_2/S_1 CI seam by deformations orthogonal to the S_2 MEP, in particular, along the symmetric CNN bending mode (see the geometrical parameters of CIs reported in Figure 3). Therefore, an ultrafast $S_2 \rightarrow S_1(n\pi^*)$ decay at N=N twisting angles that are quite far (90°) may occur.

Since the S_1 skeletal relaxed structure is quite different than the geometry of S_1/S_2 CIs reported above, some vibrations, in particular, the NN and NC stretchings and the NNC bendings, will likely absorb a large fraction of the S_2-S_1 energy difference in the $S_2 \rightarrow S_1(n\pi^*)$ decay.

Analysis of the S_1/S_0 Crossing Region. The vibrational energy excess in S_1 will be quickly distributed among all the vibrations. When this process is completed, little energy is left to the coordinates associated with isomerization (N=N twisting and NNC bendings), and the S_1 state produced via the S_2 excitation shows the same photochemical behavior as the directly excited (by $S_0 \rightarrow S_1$ absorption) S_1 state. That is, the molecules in which a complete vibrational redistribution takes place in S_1 will follow the S_1 MEP (mainly along the torsion coordinate) and reach the twisted geometry where they isomerize.

Alternatively, before vibrational redistribution is completed, molecules may intercept a seam of S_1/S_0 CIs at a variety of θ angles, whereby the decay to S_0 occurs. In fact, we have found a seam of S_1/S_0 CIs with energy close to S_2 and to the S_2/S_1 crossing region, which extends along the full $0° < \theta < 90°$ interval. This seam of S_0/S_1 CIs is characterized by a short NN bond (1.22 Å) and large NNC inversion angles and is very similar to the S_1/S_0 intersection seam of the *E* isomer.

The topology of this S_1/S_0 crossing space is substantially identical in the two isomers, and the same conclusions can be drawn as for the *E* isomer (S_1/S_0 crossing region shape in Scheme 1). In general, the CIs at *symmetric* CNN/NNC bending

Scheme 1. Topology of the S_1/S_0 Crossing Seam of the trans Isomer

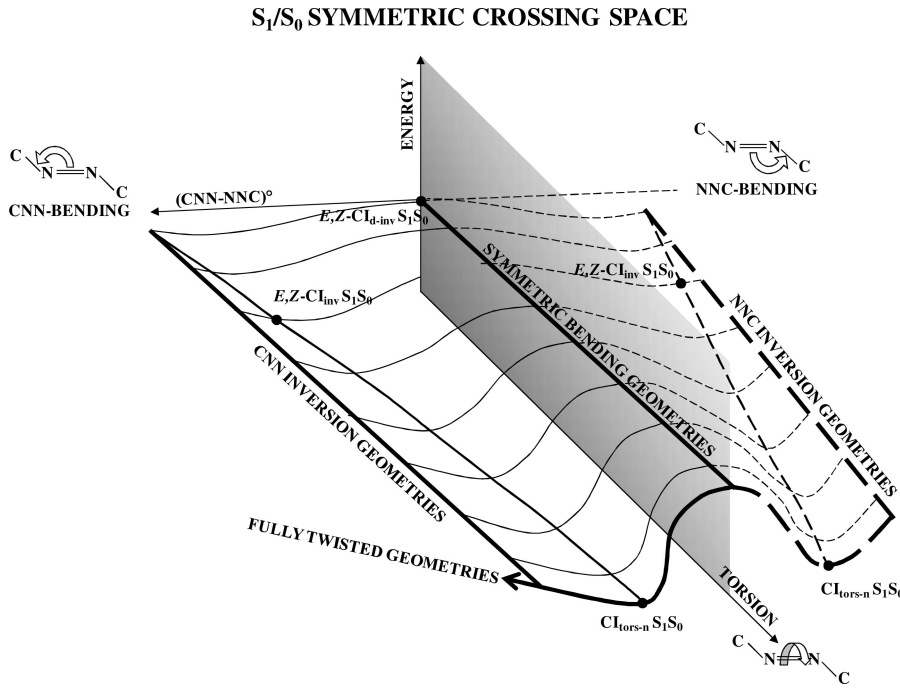

geometries have the highest energies, while lower energies are associated with *nonsymmetric* NNC and CNN bending angles. The lowest energy CIs are found for θ close to 90°.

In conclusion, the lowest S_1/S_0 CIs, found at a fully twisted N=N bond, are the only ones that are accessible to cold molecules and that may lead to isomerization. The S_1/S_0 CIs found at partial N=N torsion and lying at higher energy can be *potentially* entered by molecules decaying from higher-energy states, such as the S($\pi\pi^*$) state, and do not lead to isomerization. It is from these CIs that the smaller isomerization quantum yield observed for S($\pi\pi^*$), with respect to the S_1(nπ^*) state, follows. Anyway, starting from the *Z* isomer, the S_2/S_1 crossing seam is accessed at geometries more twisted than that for the *E* isomer. Thus, the $S_1 \rightarrow S_0$ decay is more likely to occur at larger value of the torsion angle (θ) than for the *E* isomer, and the isomerization yield will be higher.

Oscillator strength (*f*) calculations show a low-lying slightly absorbing state at both *E* and *Z* S_0 equilibrium geometries: these are the S_3 (B_u, $f = 0.07$) and S_2 (B, $f = 0.035$) benzenic states, respectively. The relaxation paths computed from the FC region (see Figures 2 and 3) clearly show that molecules excited to these states undergo a fast deactivation to the S_2(DE) state, which thereafter drives the relaxation to the twisted geometry or the internal conversion to the lower S_1(nπ^*) state in the same way as for the excitation to the $\pi \rightarrow \pi^*$ bright state.

3.3. Interpretation of Time-Resolved Spectra. In this section, we discuss the various stages of the S($\pi\pi^*$) decay by comparing the spectral features of time-resolved absorption spectra with the intensities of the absorption transitions of the S_1(nπ^*), S(DE), and S($\pi\pi^*$) computed in the CASSCF−CASPT2 scheme. We take as reference the *E* and *Z* transient spectra in the 350–650 nm range measured by Braun and co-workers.[33] Most of our discussion is limited to the *E* isomer because the information available for the *Z* isomer pertains practically only to S_1(nπ^*).

In the *E* isomer, the decay of the transient absorption induced by the S($\pi\pi^*$) excitation is represented by three exponentials with times constants of about $\tau_1 = 0.15$ ps, $\tau_2 = 0.45$ ps, and $\tau_3 = 2.7$ ps.[33] A transient species with a specific absorption spectrum[33] is associated with each of these exponentials.

The transient species with a time constant of $\tau_1 = 0.15$ ps has a spectrum showing two maxima[33] at 470 and 600 nm. The two transient spectra with lifetimes of $\tau_2 = 0.45$ ps and $\tau_3 = 2.7$ ps, which are associated with the state S_1(nπ^*),[33] assigned to vibrational relaxation within S_1(nπ^*) and to the decay of the relaxed S_1(nπ^*),[33] respectively, show very similar transient spectra both with maxima at about 400 and 530 nm.

We consider first the S($\pi\pi^*$) state, which, according to our calculations (vide supra), undergoes a fast relaxation process followed by a fast S($\pi\pi^*$)→S(DE) decay (internal conversion). We have computed the oscillator strengths, *f*, of several S($\pi\pi^*$)→S_n transitions both at the S_0 and at the S($\pi\pi^*$) equilibrium geometry, in order to distinguish the relaxation from the decay process. The most intense S($\pi\pi^*$)→S_n transitions are obtained at 590 nm (with $f = 0.09$) at the S_0 equilibrium geometry and at 485 nm (with $f = 0.03$) at the S($\pi\pi^*$) equilibrium geometry. The comparison between the computed S($\pi\pi^*$)→S_n transitions and the observed spectrum of the shortest lived (0.15 ps) transient is quite satisfactory and strengthens the assignment of this transient to the state S($\pi\pi^*$). It is interesting to note that the two bands were calculated at the S($\pi\pi^*$) and S_0 (or FC) equilibrium geometries, respectively. This implies that the decay of the 590 nm band is related to the vibrational relaxation of S($\pi\pi^*$) from the initial FC geometry, and the disappearance of the 485 nm band must be assigned to the S($\pi\pi^*$)→S(DE) decay of the relaxed S($\pi\pi^*$). Because of the limited time resolution of these measures and of the data treatment, the two processes are not resolved in time but are spectrally distinguishable.

We have computed also the intensities of the S(DE) →S_n transitions to assess whether we can identify a contribution of the doubly excited state to the observed transient absorption. The S(DE)→ S_n transitions in the proper spectral range were found to have very small oscillator strengths, with $f < 0.01$.

Scheme 2. Summary of the Photoisomerization Paths and Yields from the Lowest $\pi\pi^*$ Absorbing State Starting from the *E* (Right Side) and *Z* (Left Side) Isomers

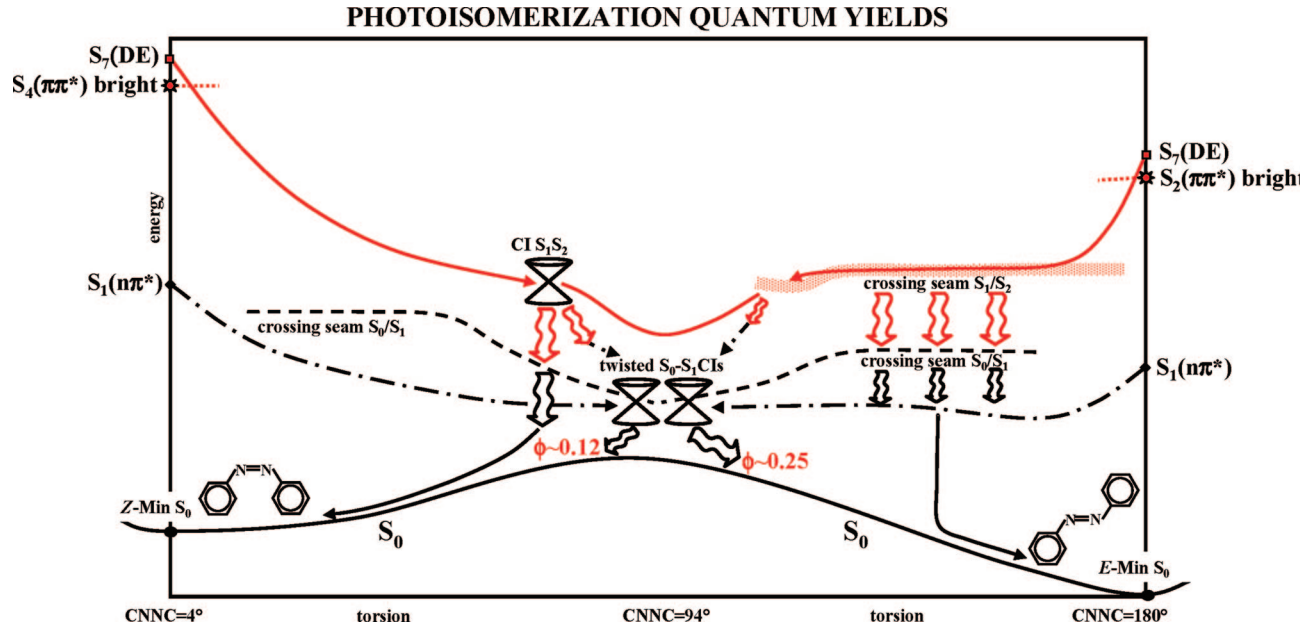

Thus, the state S(DE) is not expected to leave any trace in the transient absorption spectra.

We have computed the oscillator strengths of the $S_1(n\pi^*)\rightarrow S_n$ transitions both at the $S_1(n\pi^*)$ and S_0 (or FC) equilibrium geometries. At the latter geometry, the most intense transitions appear at 355 nm (with $f = 0.05$), 398 nm (with $f = 0.07$), and 559 nm (with $f = 0.02$). At the former geometry, the strongest transitions are found at similar wavelengths, namely, at 343 nm (with $f = 0.18$), 404 nm (with $f = 0.04$), and 622 nm (with $f = 0.02$). We note first that the $S_1\rightarrow S_n$ spectra predicted for the two geometries, namely, for the relaxation and for the decay of S_1, appear very similar. Since the shortest wavelength transition is outside the observed spectral range,[33] we consider only the two remaining transitions for the comparison. The good agreement between the computed $S_1\rightarrow S_n$ transitions and the observed transient spectra with 0.45 and 2.7 ps lifetimes supports the assignment of these transient spectra to the $S_1(n\pi^*)$ state. Interestingly, in this case, the relaxation and the decay processes are not distinguished by their spectra but only by their different time constants.

In the *Z* isomer, the decay of the transient absorption induced by the $S(\pi\pi^*)$ excitation is well described by two exponentials with lifetimes of 0.2 and 1 ps.[33] The shorter lived spectrum is structureless and flat and leaves little room to attempt an assignment to specific transitions. The longer lived spectrum shows maximum at 390 nm and a weaker feature at 550 nm.[33] The computed oscillator strengths of the $S_1(n\pi^*)\rightarrow S_n$ transitions at the S_0 (or FC) equilibrium geometry indicate that the transitions corresponding to 385 nm (with $f = 0.02$), 419 nm (with $f = 0.02$), and 651 nm (with $f = 0.02$) are the most intense in the proper energy range. Thus, assigning the computed 385 and 419 nm transitions to the observed 390 nm band and the 651 nm transition to the 550 nm band, we find a qualitative agreement. Thus, the attribution of the 1 ps transient spectrum to $S_1(n\pi^*)\rightarrow S_n$ transitions is supported by this calculation.

A different type of time-resolved spectroscopy, namely, the TRPES,[62] has been used to unravel the excited electronic states involved in the photoisomerization of Ab.[37] The TRPES study in jet-cooled *E*-Ab molecules excited to the bright $S(\pi\pi^*)$ state revealed two bands with vertical IPs of 8.6 and 9.6 eV, decaying exponentially with 0.17 and 0.42 ps time constants, respectively. The authors assigned these two transients to the decay of the bright $S(\pi\pi^*)$ state and of the B_u benzenic state $(S(2B_u)_{benz}$, which has $\pi_1\rightarrow\pi^*_{N=N}$ as dominant component; see Table 2), respectively, by comparison with the known experimental IPs of the Ab π orbitals (8.4 eV for the $\pi_{N=N}$ and 9.3 eV for the π_1 and π_2 benzenic orbitals).[63] Since the intensity of the TRPES band attributed to the benzenic state is far too intense in comparison with the relative intensity of the $S_0\rightarrow S(2B_u)_{benz}$ transition, as it can be seen from Table 2, one may wonder whether alternative interpretations for the 0.42 ps band in the TRPES spectrum can be proposed. In this respect, we note that at the $S(\pi\pi^*)$ relaxed geometry the S(DE) state has roughly the same energy as the bright $S(\pi\pi^*)$ and the benzenic states, as it is shown in Table 2. Beside the configuration $\pi_{N=N}\pi_{N=N}\rightarrow\pi^*_{N=N}\pi^*_{N=N}$, the S(DE) state contains also the configuration $\pi_2\rightarrow\pi^*_{N=N}$, which appears also in the $S(2A_g)_{benz}$ state, with an appreciable 0.45 coefficient (see Table 2). We have checked by Hartree–Fock 6-31G* basis set calculations that the two π_1 and π_2 orbitals have essentially identical energies: we found 8.19 eV for $\pi_{N=N}$, 9.16 and 9.17 eV for π_1 and π_2, respectively. Thus, the 9.6 eV TRPES band[37] may be associated with the DE state. Since the S(DE) state is promptly formed from the bright $S(\pi\pi^*)$ state and decays very fast to S_1, the 9.6 eV, 0.42 ps lifetime TRPES band is expected to have a similar intensity as the 8.6 eV, 0.17 ps band, as it is observed. If this interpretation is correct, the TRPES spectrum gives the only experimental trace of the S(DE) state.

4. Discussion

The photoisomerization of Ab upon excitation of the bright $S(\pi\pi^*)$ state has been found to occur predominantly along the

(62) Stolow, A. *Annu. Rev. Phys. Chem.* **2003**, *54*, 89.

(63) Petrachenko, N. E.; Vovna, V. I.; Furin, G. G. *J. Fluor. Chem.* **1993**, *63*, 85.

Scheme 3. Pictorial Description of the Photoisomerization Path of the *E* Isomer from the S($\pi\pi^*$) State, Including the S_1/S_0 and S_2/S_1 Crossing Seams and Showing the Most Important Coordinates[a]

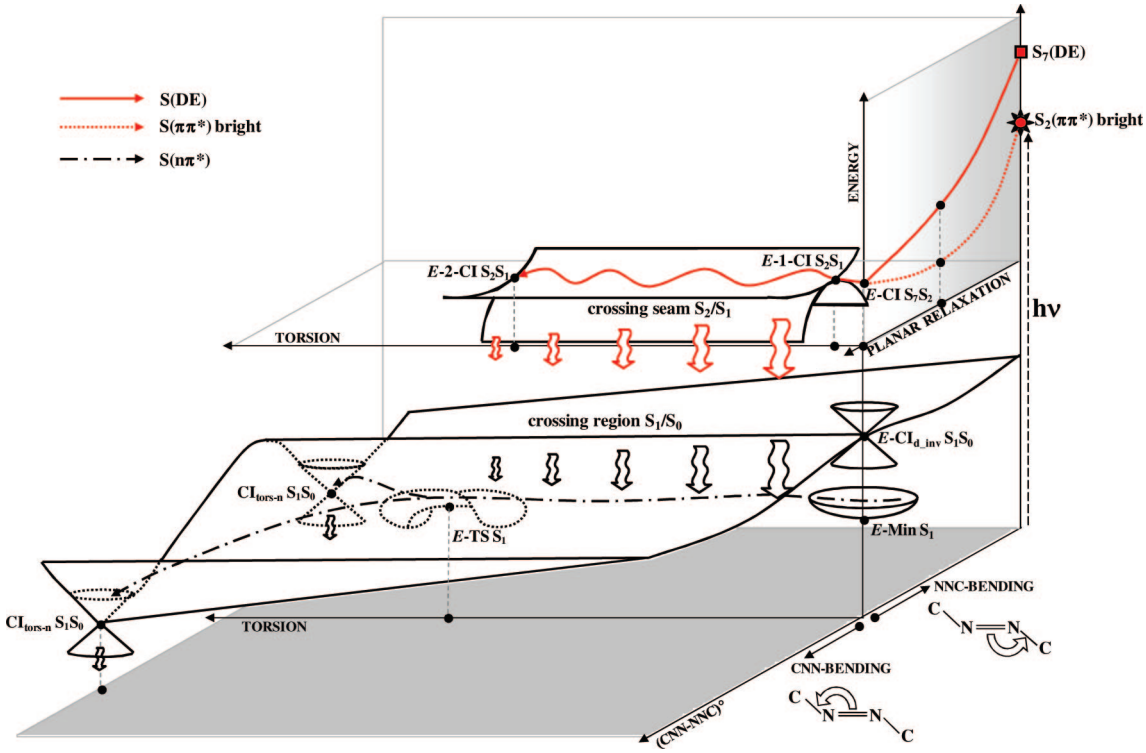

[a] While the S_2 path to the S_2/S_1 crossing region involves mainly a planar relaxation and the torsion, the S_1 relaxation involves mainly CNN bendings and the torsion.

torsion path, that is, by the same route of the $S_1(n\pi^*)$ photoisomerization as it is shown in Scheme 2.

This is not to say that the inversion coordinate is frozen and it does not play any role. In fact, the NNC and CNN angles are important parameters in defining the critical structures for the $S_1(n\pi^*)\rightarrow S_0$ decay, as it can be seen in Figures 2 and 3 and in Scheme 1. In particular, in Figure 2, one of the $S_1(n\pi^*)/S_0$ CIs (E-CI_{inv} S_1S_0), with $\theta = 120°$, CNN = 172°, and NNC = 127°, is documented. Therefore, although a fraction of photoisomerization might occur via the inversion path when a large amount of vibrational energy is available, the features of the MEPs of the relevant electronic states definitely favor the N=N torsion mechanism. A more quantitative estimate of the dominant isomerization channel in specific initial conditions could be obtained by performing MD calculations with CASSCF/CASPT2 energies, which at the moment is not feasible.

A fundamental role in the photochemistry of Ab induced by the S($\pi\pi^*$) excitation is played by the S(DE) state, based on the doubly excited configuration $\pi_{N=N}\pi_{N=N}\rightarrow\pi^*_{N=N}\pi^*_{N=N}$. This state is the necessary intermediate in promoting the conversion from the bright S($\pi\pi^*$) to the $S_1(n\pi^*)$ state, thereby ensuring that the photoisomerization process occurs and takes predominantly the torsion path from both isomers. It is interesting to note also the analogy with stilbene, where an important role in driving the photoisomerization in attributed to the $\pi\pi\rightarrow\pi^*\pi^*$ doubly excited state.[64,65]

The difference between $Z\rightarrow E$ ($\varphi \sim 0.25$) and $E\rightarrow$ ($\varphi \sim 0.12$) photoisomerization quantum yields is readily explained on the basis of the present results. Although a similar mechanism governs the photoisomerization of the *E* and *Z* isomers excited in the bright S($\pi\pi^*$) state, the calculated barrierless and steeper S(DE) MEP of the *Z* isomer, essentially along the N=N twisting coordinate, versus the gently sloped MEP of the *E* isomer, accounts for the observed higher photoisomerization yield of the $Z\rightarrow E$ with respect to the $E\rightarrow Z$. Furthermore, while in the *Z* isomer the S(DE)$\rightarrow S_1$ decay occurs via CIs in a N=N twisting region at about 65° (see Figure 3), with the torsional impulse providing the drive to move toward the twisted geometry and thereby possibly isomerize, the S(DE)$\rightarrow S_1$ decay in the *E* isomer can occur at much less twisted structures (vide supra) with a larger probability of returning via S_1/S_0 CIs to the ground-state *E* isomer.

The difference between the photoisomerization quantum yields obtained by exciting the $\pi\pi^*$ and $n\pi^*$ states, with the former always smaller than the latter, is a very specific feature of Ab photochemistry. Since we have just shown that in both isomers all the $\pi\pi^*$ photoexcited molecules are ultimately collected in the $S_1(n\pi^*)$ state (which then drives the deactivation to the ground state), the difference between the $\pi\pi^*$ and $n\pi^*$ quantum yields may appear surprising. The observed difference in the photoisomerization quantum yields can be rationalized by considering the complex S_1/S_0 crossing region described above and summarized in Schemes 3 and 4, for the *E* and *Z* isomers, respectively. In these schemes, we also depict the energy dependence of the relevant electronic states on the skeletal deformations (including CNN and NNC bendings) and the torsion coordinate and distinguish their contribution.

Following the excitation on the bright S($\pi\pi^*$) state and the prompt S($\pi\pi^*$)$\rightarrow$S(DE) conversion, the S(DE)$\rightarrow S_1$ decay occurs at energies that are higher than the S_1/S_0 crossing region for a

(64) Orlandi, G.; Siebrand, W. *Chem. Phys. Lett.* **1975**, *30*, 352.
(65) Orlandi, G.; Palmieri, P.; Poggi, G. *J. Am. Chem. Soc.* **1979**, *101*, 3492.
(66) Quenneville, J.; Martinez, T. J. *J. Phys. Chem. A* **2003**, *107*, 829.

Scheme 4. Pictorial Description of the Photoisomerization Path of the *Z* Isomer from the S($\pi\pi^*$) state, Including the S_0/S_1 and S_2/S_1 Crossing Seams and Showing the Most Important Coordinates[a]

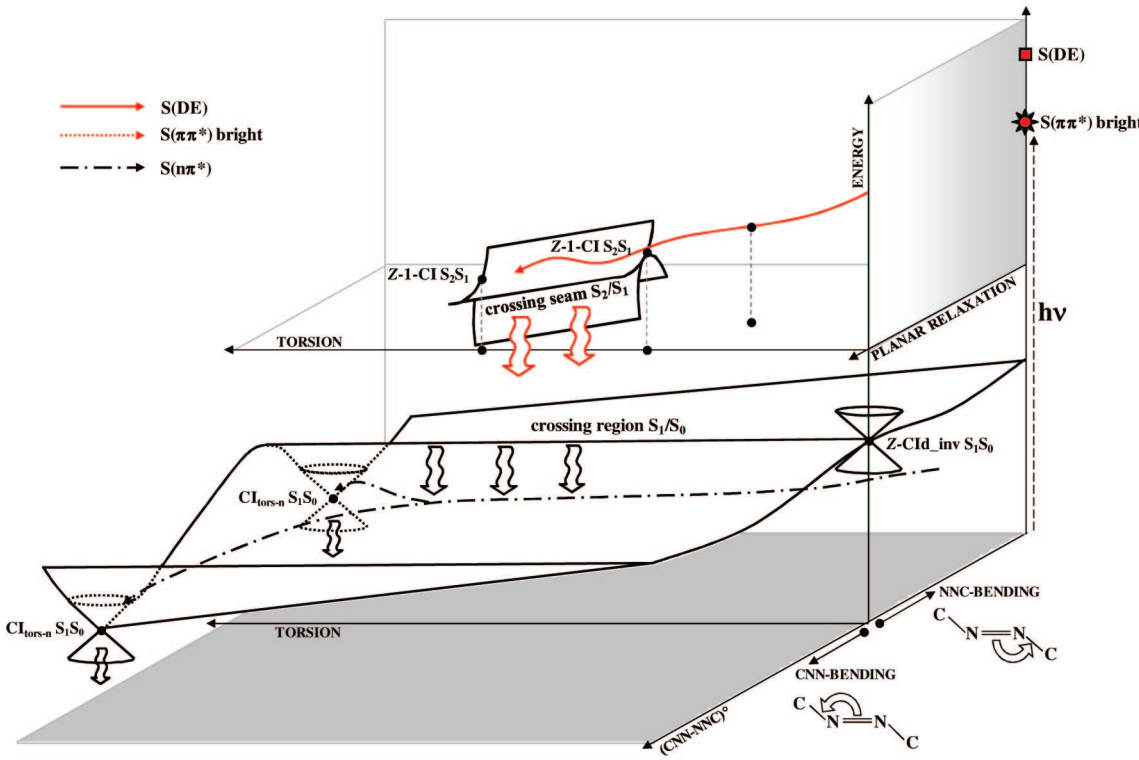

[a] While the S_2 path to the S_2/S_1 crossing region involves mainly a planar relaxation and the torsion, the S_1 relaxation involves mainly CNN bendings and the torsion.

range of twisting angles. Thus, after the $S_2 \rightarrow S_1$ conversion, molecules on the S_1 state may enter the S_1/S_0 crossing region also at partially twisted geometries, i.e. on the reactant side, and well before reaching the lowest energy CIs at the fully twisted $N=N$ bond (as shown in Scheme 3 and 4). This should induce the decay to the ground state, leading preferentially to reactant formation because of the S_0 shape along the torsion coordinate (see Scheme 2): it leads to a decrease of the photoisomerization quantum yield. On the contrary, following the excitation on the S_1 state, molecules have not enough energy to intercept the S_1/S_0 crossing region at partially twisted geometries and can only relax to the twisted geometry from where the branched decay to S_0 leads to *E*/*Z* isomerization. This explains why the photoisomerization yields from S_1 excitation are higher than the yields from the bright S($\pi\pi^*$) state.

The relative probabilities of intercepting the S_1/S_0 crossing region at partially twisted geometries and of reaching the lowest energy CIs at the fully twisted geometry can be assessed quantitatively only by molecular dynamic simulations, as recently shown by Persico and co-workers,[24,43] which is outside of the scope of this work.

To explain the two bands appearing in the TRPES spectra, Stolow and co-workers[37] suggested that in the excitation of the $\pi\pi^*$ bright state a fraction of the molecules is excited to the benzenic B_u state and suggested that these molecules decay to S_0 bypassing the S_1 state and without isomerization, thus explaining the smaller quantum yield of photoisomerization in S($\pi\pi^*$) than in S_1(nπ^*). We note that the oscillator strength ratio of the benzenic over the bright state is roughly 0.1, according to different calculations[37,61] and the present work (see Table 2). Thus, the effect of the benzenic state absorption would be very minor. Furthermore, as shown in Figure 2, the molecules reaching the benzenic state can decay efficiently only via the S(DE) state and, therefore, they would follow the same fate as the molecules excited to the bright state. Finally, we note that the TRPES band at 9.6 eV decaying with a 0.42 ps lifetime[37] can be associated also with the S_2(DE) state because of its benzenic component (see Table 2) and for its intensity and likely reflects the decay of the S_2(DE) state.

An interesting and related issue concerns the mechanism of photoisomerization of sterically hindered azobenzenes, such as the Ab-phanes[3,4] and of azobenzene-capped crown ether.[22] In these compounds, the Kasha rule is obeyed and the quantum yields of photoisomerization in S_1 and S_2 are the same and are qualitatively equal to the quantum yield of Ab in S_1, in contrast with the results obtained for the free Ab. The original interpretation[3,4,22] of these observations is based on the following assumptions: (a) photoisomerization in the free Ab molecules occurs in S_1(nπ^*) and S($\pi\pi^*$) along the inversion and in the torsion route, respectively, (b) the torsion mechanism is forbidden in hindered Ab for sterical reasons. It follows that in these molecules isomerization can take only the inversion path and the S($\pi\pi^*$) can return to S_0 only via S_1(nπ^*),[3,4,22] and that the isomerization quantum yield is the same in the two states. Thus, the results for the hindered Ab were taken as a support for the mechanistic assumption that photoisomerization in the free Ab molecules occurs in S_1(nπ^*) and S($\pi\pi^*$) along the inversion and the torsion route, respectively.

The above assumptions are not supported by recent experimental and theoretical findings. As already noted, the feasibility of the torsion mechanism in the Ab-phanes is underscored by the experiments of Tanner and Wennerstrom[28] who showed that also stilbeno-phanes, for which obviously the inversion coordinate is not available, do isomerize. This underlines the notion

that steric constraints are usually not rigid but have some degree of flexibility, which is related to the soft potentials of some coordinates. Moreover, recent time-resolved studies of the *hindered* crown ether capped *E*-Ab (*E*-Ab1) and of *free E*-Ab chemically similar to *E*-Ab1 (containing two aminocarbonyl groups on the two rings) showed almost the same S_1 biexponential decay[47] (with $\tau_1 \approx 1$ ps and $\tau_2 \approx 20$ ps), while the corresponding parameters of *E*-Ab are $\tau_1 \approx 3$ ps and $\tau_2 \approx 2.6$ ps.[29–31] These results on the crown ether capped Ab underscore the fact that *chemical effects* always accompany the *steric constraints* in the intended hindered derivatives.

The *E*-Ab1 derivative together with its parent *E*-Ab were studied by Car–Parrinello molecular dynamics method to assess the mechanism of isomerization in S_1 and the effect of the steric constraints in the capped *E*-Ab.[45] The results showed that isomerization in S_1 follows the N=N torsion in both compounds,[45] confirming earlier results by Ciminelli et al. for *E*-Ab and Ab-phanes[24,44,46] where it is shown that the $S_1 \rightarrow S_0$ deactivation routes for both $n\pi^*$ and $\pi\pi^*$ excitations involve N=N central bond torsions. More specifically, it is shown that trajectories in hindered Ab do not cross structure regions characterized by large values of NNC angles. Thus, according MD trajectories,[44–46] NNC deformations rather than N=N torsion appear surprisingly to be contrasted by steric constraints.

A natural explanation for the non-Kasha behavior of free Ab and for the Kasha behavior of hindered Ab emerges readily from the effects indicated by MD calculations of steric constraints[44–46] and from our calculation. In fact, we find that, for the free *E*-Ab excited to the bright $S(\pi\pi^*)$ state, the higher-energy S_1/S_0 CIs that occur far from twisted geometries, which lead to $S_2(DE) \rightarrow S_1 \rightarrow S_0$ conversion without isomerization (causing the non-Kasha behavior), *require large values of the NNC and CNN angles* (vide supra). On the contrary, the topology of the S_1/S_0 crossing region (Scheme 1) shows that the low-lying fully twisted CIs ($CI_{tors\text{-}n}$ S_1S_0) are characterized by the lowest CNN and NNC angles. Since large NNC angles are inhibited in a sterically hindered Ab but are permitted in free Ab, the $S_2(DE) \rightarrow S_1 \rightarrow S_0$ conversion is compatible with vertical $S_1 \rightarrow S_0$ decay with loss of photoisomerization yield in the latter but can occur only at substantially twisted geometries, whereby the photoisomerization yield is as large as that for the excitation on S_1 in the former. These conclusions support previous simulations on azobenzenophanes.[44,46]

Such consideration is useful also for the applications; for example, Ab-type systems in which the opening of NNC angles is hindered are good candidates for high-yield photoisomerization-based molecular machines.

One may be surprised that two different approaches such as Carr−Parrinello and semiempirical CAS give the same mechanistic picture of Ab photoisomerization in S_2. It is easier to compare the latter method with ours: in both cases, a key role is played by the A state as the photoreaction intermediate. The nature of this state is not clarified by Persico and co-workers.[44,46] In our calculations, it is clearly associated with the DE configuration, and we indicate that the experimental signature of this state is to be found in the TRPES spectra.

5. Conclusions

In this work, we have analyzed the isomerization routes of *E*-Ab and *Z*-Ab in the bright $S(\pi\pi^*)$ state by using high-level quantum chemical methods. We have clarified the decay path and the mechanism of photoisomerization of the $S(\pi\pi^*)$ state and have explained the lower cis–trans isomerization quantum yields observed for $S(\pi\pi^*)$ excitation than for $S_1(n\pi^*)$ excitation for the isolated molecule. In the following we summarize the main results.

The photoisomerization process upon excitation of the $S(\pi\pi^*)$ state follows the torsion path, that is, the same path found earlier for the S_1 and T_1 excited states.[25] In the $S(\pi\pi^*)$ photoisomerization process, a fundamental role is played by the S(DE) state, which is based on the doubly excited configuration $\pi_{N=N}$ $\pi_{N=N} \rightarrow \pi^*_{N=N}\pi^*_{N=N}$. The MEP of this state, having its minimum at the twisted geometry, drives the photoisomerization process along the torsion path and, simultaneously, the fast internal conversion to $S_1(n\pi^*)$ for both isomers. The S(DE) state is the necessary intermediate bringing about the conversion from the bright $S(\pi\pi^*)$ state to the $S_1(n\pi^*)$ state, and we suggest that TRPES spectra provide the first observation of this state.

The lower photoisomerization quantum yields from $S(\pi\pi^*)$ than from $S_1(n\pi^*)$ is the consequence of the accessible $S(DE) \rightarrow S_1$ and $S_1 \rightarrow S_0$ CIs located *at near planar structures*, which require large NNC angles, through which the conversion to the ground state can take place at reactant geometries. This finding agrees with the proposal of Tahara and co-workers and provides details about the path through which it materializes.

The normal behavior of the hindered Ab is due to the circumstance that the $S_1 \rightarrow S_0$ CIs at near planar structures are not accessible because the very hindrance forbids the large NNC angles that are required.[45] Thus, the very CIs that are responsible of the non-Kasha behavior of Ab are not accessible in the hindered Ab.

Acknowledgment. Support by funds from MURST PROGETTO PRIN E.F. 2005 Prot 2005034397 "Trasferimenti di energia e di carica a livello molecolare" is gratefully acknowledged.

Supporting Information Available: Cartesian coordinates of all the optimized structures discussed in the text, absolute energy (in Hartrees) of all calculated structures (Table S1 and Table S2), complete refs 55 and 56. This material is available free of charge via the Internet at http://pubs.acs.org.

JA710275E